Control and Cybernetics
vol. **54** (2025) No. 2
pages: 157-204
DOI: 10.2478/candc-2025-0006

Nonlinear optimal control for two cable-driven 3-DOF robotic cranes*

by

Gerasimos G. Rigatos [a,*], Farouk Zouari [b], Masoud Abbaszadeh [c], Mohammed Al-Numay [d] and Pierluigi Siano [e]

[a]Unit of Industrial Automation, Industrial Systems Inst.
26504 Patras, Greece
*corresponding author: grigat@ieee.org
[b]Laboratoire d' Automatique, Université de Tunis El Manar,
1068 Tunis, Tunisie 12065,
farouk.zouari@enit.utm.tn
[c]Department of ECS Engineering, Rensselaer Polytechnic Institute,
12065 New York, USA
masouda@ualberta.ca
[d]Department of Electrical Engineering, King Saud University,
Riyadh 11421, Saudi Arabia
alnumay@ksu.edu.sa
[e]Department of Management and Innovative Systems, University of Salerno,
Fisciano 84084, Italy
psiano@unisa.it

Abstract: The article is concerned with the nonlinear optimal control problem of two cable-driven 3-DOF robotic cranes. Such cranes can be used in ship maintenance and repair. These are underactuated robotic systems comprising a 2-cable driven cart with a payload suspended from it. Such robotic mechanisms have three degrees of freedom and can move in the entire 2D vertical plane. Using Euler-Lagrange analysis the state-space model of the two cable-driven 3-DOF robotic crane is obtained. It is also proven that this dynamic model is differentially flat. Next, to solve the associated nonlinear optimal control problem, the dynamic model of the two cable-driven 3-DOF robotic crane undergoes approximate linearization around a temporary operating point that is recomputed at each time-step of the control method. The linearization relies on Taylor series expansion and on the associated Jacobian matrices. For

*Submitted: December 2024; Accepted: September 2025

the linearized state-space model of the crane an optimal (H-infinity) feedback controller is designed. This controller stands for the solution to the nonlinear optimal control problem under model uncertainty and external perturbations. To compute the controller's feedback gains an algebraic Riccati equation is repetitively solved at each iteration of the control algorithm. The stability properties of the control method are proven through Lyapunov analysis. The proposed nonlinear optimal control approach achieves fast and accurate tracking of reference setpoints under moderate variations of the control inputs. Besides, the method avoids change of state variables and state-space model transformations and the control inputs it computes are applied directly on the initial nonlinear state-space model of the crane.

Keywords: two cable-driven 3-DOF robotic crane, ship repair, underactuated crane, differential flatness properties, nonlinear H-infinity control, Taylor series expansion, Jacobian matrices, Riccati equation, global stability.

1. Introduction

Cable-driven cranes are widely used in industry and in applications, requiring the crane to operate in a large work-space (Mojallizadeh, Brogliato and Prieur, 2023; Harandi, Khalipour and Taghirad, 2023; Harandi and Taghirad, 2021; Zhu et al., 2023; Hosseini, Khalipour and Taghirad, 2021). Cable-driven robots are light, easy to install and maintain electromechanical systems, which are characterized by large payload transfer capability (Bhadure, Venkatesh and Kazi, 2012; Étienne et al., 2022; Gogte et al., 2014). However, control of such robots exhibits difficulties, due to their strongly nonlinear dynamic model and underactuation (Nurkanovic et al., 2023; Brogliato, 2023; Choukchou-Braham et al., 2014). In this article, a specific type of cable-driven robots is examined, which is the two cable-driven 3-DOF robotic crane (Bucieri, Mullhaupt and Bonvin, 2005; Kazi et al., 2008). Such a crane consists of a cart, which is suspended in the vertical plane by two cables. Each cable is connected to an electric motor. When varying the motors' turn speed and torque, the length and the tension of the cables also changes. A payload is attached to the cart with a link of constant length. By changing the motor's torque, the position of the cart in the vertical plane changes and the payload is moved to a different position. The cart and payload system performs a 3-DOF motion, which is defined by the cartesian coordinates of the cart and by the swing angle of the payload.

So far, there have been several attempts to solve the nonlinear control problem for the two cable-driven 3-DOF robotic crane (Harandi, Namvar and Taghirad, 2023; Romero et al., 2022; Romero and Ortega, 2015; Mehra et al., 2017). One can distinguish, for instance, methods of global linearization-based control (Buccieri et al., 2005; Kazi et al., 2009). There exist also results on model predictive control of these robotic cranes (Mejari et al., 2014; Kamath, Kazi and Singh, 2010). One can note also several Lyapunov theory-based and energy-based control schemes (Harandi and Taghirad, 2021, 2023; Romero et al., 2018; Mehra et al., 2012). Addditional references on underactuated cable-driven robots can be found in Lucarini, Ida and Carricato (2025); Huang et al. (2016, 2022); Ida, Bruckmann and Carricato (2019); Seifired (2013); Barabazzo et al. (2017). Besides, additional references on nonlinear control of cable-driven robots can be seen in Pivo, Richiedei and Trevisani (2025); Gamboa Penalosa (2025); Li et al. (2025); Sun et al. (2025); Li, Shang and Zhang (2023); Zhang, Shang and Cong (2025).

In this article a novel nonlinear optimal control method is proposed for the dynamic model of two cable-driven 3-DOF robotic cranes (Rigatos and Busawon, 2018; Rigatos, Abbaszadeh and Siano, 2022; Rigatos and Karapanou, 2020; Rigatos et al., 2024). Such cranes can be used in ship maintenance and repair. To implement this method, the dynamic model of the robotic crane is formulated first using Euler-Lagrange analysis (Rigatos and Busawon, 2018). Differential flatness properties are also proven for this dynamical system (Rigatos, 2016). Next, the model of the robotic crane undergoes approximate linearization with the use of first-order Taylor series expansion and through the computation of the associated Jacobian matrices (Rigatos and Tzafestas, 2007; Rigatos and Zhang, 2009; Basseville and Nikiforov, 1993). The linearization takes place at each sampling instance around the temporary operating point (x^*, u^*), where x^* is the present value of the system's state vector and u^* is the last sampled value of the control inputs vector. The modelling error, which is due to the truncation of higher-order terms from the Taylor series, is considered to be a perturbation, which is asymptotically compensated by the robustness of the control algorithm. For the approximately linearized model of the system a stabilizing H-infinity feedback controller is designed. This controller represents a min-max differential game taking, place between: (i) the control inputs, which try to minimize the quadratic term of the state vector's tracking error, and (ii) the model uncertainty and external perturbation terms, which try to maximize this cost function.

To select the gains of the H-infinity controller, an algebraic Riccati equation has to be repetitively solved at each time-step of the control algorithm. The global stability properties of the control scheme are proven through Lyapunov analysis. First, it is demonstrated that the control loop satisfies the H-infinity tracking performance criterion, which signifies elevated robustness against model uncertainties and external perturbations (Rigatos and Karapanou, 2020; Toussaint, Basar and Bullo, 2000). Moreover, under moderate conditions it is proven that the control loop is globally asymptotically stable. To implement state estimation-based control without the need of measuring the entire state vector of the controlled system, the H-infinity Kalman Filter is used as a robust state estimator (Rigatos and Busawon, 2018; Rigatos and Karapanou, 2020). The method achieves fast and accurate tracking of reference setpoints by the state variables of the robotic crane. Besides, it achieves all control objectives for this robotic crane without the need for state-space model transformations and without the need for change of state variables.

Compared to other attempts that aimed at solving the nonlinear optimal control problem for complex dynamical systems, the article's nonlinear optimal control method is significantly novel. Whereas in other control methods linearization is performed at points of the desirable trajectory, in the article's approach linearization takes place at each sampling instance around the present position of the system. This allows to keep the span of the Taylor series expansion small and the associated modelling error negligible. The article uses also a new Riccati equation for computing the feedback gains of the H-infinity controller, while the method's Lyapunov stability analysis is a genuine finding. Compared to the LPV control method, the article's control approach is addressed to a class of systems, which can be written in the Linear Parameter Varying form, while it does not need, either, the solution of State Dependent Riccati equations (SDREs). Compared to methods, which try approximating the Hamilton-Jacobi-Bellman (HJB) equation with Galerkin series, the article's approach is computationally simpler and is accompanied by a global stability proof.

The structure of the article is as follows: In Section 2, the dynamic model of the two cable-driven 3-DOF robotic crane is given. Differential flatness properties for the crane's model are proven. In Section 3, the dynamic model of the robotic crane undergoes approximate linearization with the use of first-order Taylor series expansion and through the computation of the system's Jacobian matrices. In Section 4, an H-infinity feedback controller is designed for the robotic crane. In Section 5, the global stability properties of the control method are proven through Lyapunov analysis. In Section 6 the simulation tests are presented. Finally, in Section 7, concluding remarks are stated.

2. Dynamic model of the two cable-driven 3-DOF robotic crane

2.1. State-space model of the robotic crane

The diagram of the two cable-driven 3-DOF robotic crane is given in Fig. 1. Such cranes can be used in ship maintenance and repair, for instance in painting or cleaning tasks of the ship's external surfaces. The robotic crane consists of a cart, which is moved on a 2D xy-plane with the use of two strings. The winding or loosening of the cables is performed by two motors, which also vary the tension of the cables. The position of the cart in the xy-plane is denoted as (x_R, y_R). The position of the left motor is denoted as (x_a, y_a), while the position of the right motor is represented as (x_b, y_b). The mass of the cart is M. The length of the cable that connects the cart with the left motor is denoted as L_1, while the length of the cable, which connects the cart with the right motor is denoted as L_2. Besides, a load of mass m is suspended from the cart using an unactuated link of length L_3. The angle, which is formed between the OX horizontal axis and the cable that connects the cart with the left motor, is denoted as a_1. The angle, which is formed between the OX horizontal axis and the cable that connects the cart with the right motor, is denoted as a_2.

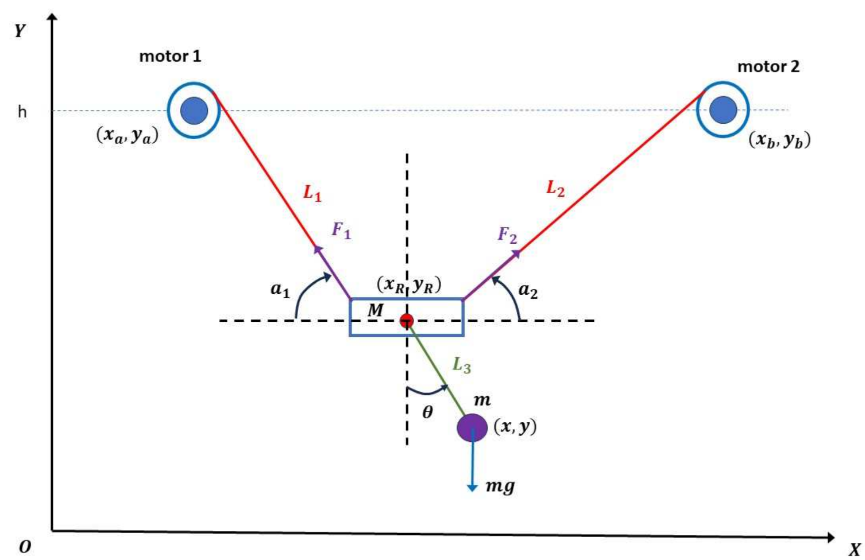

Figure 1. Diagram of the two cable-driven 3-DOF robotic crane

The moment of inertia of the left motor is I_a, while the moment of inertia of the right motor is I_b. Both motors are placed at a height along the OY axis, which is equal to h. The cables are considered to be massless and inelastic. The link, which connects the load of mass m to the cart is not subject to deformation, either. The parameters, which describe the motion of the crane, constitute the parameters vector $[x_R, y_R, \theta]^T$, while the control objective is to make this vector converge fast to the desirable value $[x_{R,d}, y_{R,d}, \theta_d]^T$ under minimal dispersion of energy by the two motors.

Using trigonometric relations, the following geometric constraints are formulated:

$$\begin{array}{l}(x_a - x_R)^2 + (y_a - y_R)^2 = L_1^2 \\ (x_b - x_R)^2 + (y_b - y_R)^2 = L_2^2 \ .\end{array} \tag{1}$$

In order to perform the Euler-Lagrange analysis for the robotic crane, its kinetic and dynamic energy are computed first. The position of the cart is (x_R, y_R), thus the associated velocity is $(\dot{x}_R, \dot{y}_R)$. The position of the payload is $(x_R + L_3 sin(\theta), y_R - L_3 cos(\theta))$ and the associated velocity is $(\dot{x}_R + L_3 cos(\theta)\dot{\theta}, \dot{y}_R + L_3 sin(\theta)\dot{\theta})$.

The dynamic model of the system will be defined using Euler-Lagrange analysis (see Rigatos and Busawon, 2018). The kinetic energy of the cart is

$$K_c = \tfrac{1}{2} M(\dot{x}_R^2 + \dot{y}_R^2). \tag{2}$$

The kinetic energy of the load is

$$K_L = \tfrac{1}{2} m[((\dot{x}_R + L_3 cos(\theta)\dot{\theta})^2 + (\dot{y}_R + L_3 sin(\theta)\dot{\theta}))^2] \ . \tag{3}$$

The aggregate kinetic energy of the crane is

$$\begin{array}{l}K = K_c + K_L \Rightarrow K = \dfrac{1}{2} M(\dot{x}_R^2 + \dot{y}_R^2) + \\ + \dfrac{1}{2} m[(\dot{x}_R + L_3 cos(\theta)\dot{\theta})^2 + (\dot{y}_R + L_3 sin(\theta)\dot{\theta})^2],\end{array} \tag{4}$$

which, after intermediate operations and regrouping of terms, gives

$$\begin{array}{l}K = \dfrac{1}{2}(M+m)\dot{x}_R^2 + \dfrac{1}{2}(M+m)\dot{y}_R^2 + \\ + m\dot{x}_R L_3 cos(\theta)\dot{\theta} + m\dot{y}_R L_3 sin(\theta)\dot{\theta} + \dfrac{1}{2} m L_3^2 \dot{\theta}^2.\end{array} \tag{5}$$

By defining vector $q = [x_R, y_R, \theta]^T$ and vector $\dot{q} = [\dot{x}_R, \dot{y}_R, \dot{\theta}]^T$, the kinetic energy of the crane can be written down in matrix form as

$$\begin{array}{l}K = \dfrac{1}{2}\dot{q}\tilde{M}q^T \Rightarrow K = \\ \dfrac{1}{2}\left(\dot{x}_R, \dot{y}_R, \dot{\theta}\right)\begin{pmatrix}(M+m) & 0 & mL_3 cos(\theta) \\ 0 & (M+m) & mL_3 sin(\theta) \\ mL_3 cos(\theta) & mL_3 sin(\theta) & mL_3^2\end{pmatrix}\begin{pmatrix}\dot{x}_R \\ \dot{y}_R \\ \dot{\theta}\end{pmatrix}.\end{array} \tag{6}$$

Next, the potential energy of the crane, consisting of the potential energy of the cart and the potential energy of the payload, is found to be

$$P = Mgy_R + mg(y_R - L_3 cos(\theta)) \ . \tag{7}$$

The Lagrangian of the crane is given by

$$L = K - P \Rightarrow L = \frac{1}{2}(M+m)\dot{x}_R^2 + \frac{1}{2}(M+m)\dot{y}_R^2 +$$
$$+ m\dot{x}_R L_3 cos(\theta)\dot{\theta} + m\dot{y}_R L_3 sin(\theta)\dot{\theta} + \frac{1}{2}mL_3^2\dot{\theta}^2 -$$
$$-Mgy_R - mg(y_R - L_3 cos(\theta)). \tag{8}$$

The forces, which are exerted on the robotic crane are the tensions of the two strings F_1 and F_2, while there is no torque. By applying Euler-Lagrange analysis, one obtains:

$$\frac{\partial}{\partial t}\frac{\partial L}{\partial \dot{q}_1} - \frac{\partial L}{\partial q_1} = F_1 \tag{9}$$

$$\frac{\partial}{\partial t}\frac{\partial L}{\partial \dot{q}_2} - \frac{\partial L}{\partial q_2} = F_2 \tag{10}$$

$$\frac{\partial}{\partial t}\frac{\partial L}{\partial \dot{q}_3} - \frac{\partial L}{\partial q_3} = 0. \tag{11}$$

From Eq. (9) and after computing the related partial derivatives of the Lagrangrian, one gets:

$$(M+m)\ddot{x}_R - mL_3 sin(\theta)\dot{\theta}^2 + mL_3 cos(\theta)\ddot{\theta} = F_1 \tag{12}$$
$$(M+m)\ddot{y}_R + mL_3 cos(\theta)\dot{\theta}^2 + mL_3 sin(\theta)\ddot{\theta} - (M-m)g = F_2 \tag{13}$$
$$m\ddot{x}_R L_3 cos(\theta) + m\ddot{y}_R L_3 sin(\theta) + mL_3^2\ddot{\theta} + mgL_3 sin(\theta) -$$
$$- m\dot{x}_R L_3 sin(\theta)\dot{\theta} + m\dot{y}_R L_3 cos(\theta)\dot{\theta} = 0. \tag{14}$$

In Eq. (14) the terms, which appear in the last row are zero, meaning that there is

$-m\dot{x}_R L_3 sin(\theta)\dot{\theta} + m\dot{y}_R L_3 cos(\theta)\dot{\theta} = 0$ or $mL_3\dot{\theta}[-\dot{x}_R sin(\theta) + \dot{y}_R cos(\theta)] = 0$.

Actually, it holds that

$-\dot{x}_R sin(\theta) + \dot{y}_R cos(\theta) = 0$.

This is obtained after considering a body-fixed frame for expressing the velocity of the load and knowing that the velocity of the load along the vertical axis of this frame is 0. Indeed, the transformation of the velocities vector of the load from the inertial reference frame to the body-fixed frame, gives

$$\begin{pmatrix} v_1 \\ 0 \end{pmatrix} = \begin{pmatrix} cos(\theta) & sin(\theta) \\ -\sin(\theta) & cos(\theta) \end{pmatrix} \begin{pmatrix} \dot{x}_R + L_3 cos(\theta)\dot{\theta} \\ \dot{y}_R + L_3 sin(\theta)\dot{\theta} \end{pmatrix}, \tag{15}$$

out of which one obtains

$$\begin{array}{c} -sin(\theta)[\dot{x}_R + L_3 cos(\theta)\dot{\theta}] + cos(\theta)[\dot{y}_R + L_3 sin(\theta)\dot{\theta}] = 0 \\ \Rightarrow - \dot{x}_R sin(\theta) + \dot{y}_R cos(\theta) = 0. \end{array} \tag{16}$$

Consequently, from Euler-Lagrange analysis, the equations of the system's dynamics become

$$(M+m)\ddot{x}_R + 0\ddot{y}_R - mL_3 sin(\theta)\dot{\theta}^2 + mL_3 cos(\theta)\ddot{\theta} = F_1 \tag{17}$$

$$0\ddot{x}_R + (M+m)\ddot{y}_R + mL_3 cos(\theta)\dot{\theta}^2 + mL_3 sin(\theta)\ddot{\theta} - (M-m)g = F_2 \tag{18}$$

$$m\ddot{x}_R L_3 cos(\theta) + m\ddot{y}_R L_3 sin(\theta) + mL_3^2\ddot{\theta} + mgL_3 sin(\theta) = 0. \tag{19}$$

In matrix form, the dynamic model of the two cable-driven 3-DOF robotic crane is written as:

$$\begin{pmatrix} (M+m) & 0 & (mL_3cos(\theta)) \\ 0 & (M+m) & (mL_3sin(\theta)) \\ (mL_3cos(\theta)) & (mL_3sin(\theta)) & mL_3^2 \end{pmatrix} \begin{pmatrix} \ddot{x} \\ \ddot{y} \\ \ddot{\theta} \end{pmatrix} +$$

$$\begin{pmatrix} -(mL_3sin(\theta))\dot{\theta}^2 \\ (mL_3cos(\theta))\dot{\theta}^2 \\ 0 \end{pmatrix} + \begin{pmatrix} 0 \\ 0 \\ mgL_3cos(\theta) \end{pmatrix} = \begin{pmatrix} F_1 \\ F_2 \\ 0 \end{pmatrix}. \tag{20}$$

Using the fact that $q =]x_R, y_R, \theta]^T$, this is a dynamic model of a robot with the inertia matrix $M(q) \in R^{3\times 3}$, the Coriolis forces vector $C(q,\dot{q}) \in R^{3\times 1}$, gravitational forces vector $G(\theta) \in R^{3\times 1}$, and external (control input) forces/torques vector $\tau \in R^{3\times 3}$. This dynamic model can be written down in the concise form as

$$M(q)\ddot{q} + C(q,\dot{q}) + G(q) = \tau\ . \tag{21}$$

The inverse of the inertia matrix $M(q)$ is computed as follows:

$$M(q)^{-1} = \tfrac{1}{detM} \begin{pmatrix} M_{11} & -M_{12} & M_{13} \\ -M_{21} & M_{22} & -M_{23} \\ M_{31} & -M_{32} & M_{33} \end{pmatrix} \tag{22}$$

where the sub-determinants of $M(q)$ are:

$$M_{11} = (M+m)mL_3^2 - (ML_3 sin(\theta))^2,\ M_{12} = -(mL_3)^2 sin(\theta)cos(\theta),$$

$$M_{13} = -(M+m)(mL_3 cos(\theta)),\ M_{21} = -(mL_3)^2 sin(\theta)cos(\theta),$$

$$M_{22} = (M+m)mL_3^2 - (mL_3 cos(\theta)^2),\ M_{23} = (M+m)(mL_3 cos(\theta)),$$

$$M_{31} = -(M+m)(mL_3 cos(\theta)),\ M_{32} = (M+m)(mL_3 sin(\theta))$$

and $M_{33} = (M+m)^2$

while the determinant of $M(q)$ is $detM = (M+m)M_{11} + (mL_3 cos(\theta))M_{13}$.

The Coriolis forces vector is written down as $C = [C_1, C_2, 0]^T$ and the gravitational forces vector as $G = [0, 0, G_3]^T$. Thus, after some intermediate operations, the dynamic model of the robotic crane is expressed as

$$\begin{pmatrix} \ddot{x}_R \\ \ddot{y}_R \\ \ddot{\theta} \end{pmatrix} = -\frac{1}{detM} \begin{pmatrix} M_{11} & -M_{21} & M_{31} \\ -M_{12} & M_{22} & -M_{32} \\ M_{13} & -M_{23} & M_{33} \end{pmatrix} \begin{pmatrix} C_1 \\ C_2 \\ G_3 \end{pmatrix} + \\ + \frac{1}{detM} \begin{pmatrix} M_{11} & -M_{21} & M_{31} \\ -M_{12} & M_{22} & -M_{32} \\ M_{13} & -M_{23} & M_{33} \end{pmatrix} \begin{pmatrix} F_1 \\ F_2 \\ 0 \end{pmatrix}, \tag{23}$$

which finally gives

$$\begin{pmatrix} \ddot{x}_R \\ \ddot{y}_R \\ \ddot{\theta} \end{pmatrix} = \begin{pmatrix} \frac{-M_{11}C_1 + M_{21}C_2 - M_{31}G_3}{detM} \\ \frac{M_{12}C_1 - M_{22}C_2 + M_{32}G_3}{detM} \\ \frac{-M_{13}C_1 + M_{23}C_2 - M_{33}G_3}{detM} \end{pmatrix} + \frac{1}{detM} \begin{pmatrix} \frac{M_{11}}{detM} & -\frac{M_{21}}{detM} \\ -\frac{M_{12}}{detM} & \frac{M_{22}}{detM} \\ \frac{M_{13}}{detM} & -\frac{M_{23}}{detM} \end{pmatrix} \begin{pmatrix} F_1 \\ F_2 \end{pmatrix}. \tag{24}$$

Next, the state vector of the robotic crane is defined as $x = [x_1, x_2, x_3, x_4, x_5, x_6]^T$ or $x = [x_R, \dot{x}_R, y_R, \dot{y}_R, \theta, \dot{\theta}]^T$, and the control inputs vector is defined as $u = [u_1, u_2]^T$ or $u = [F_1, F_2]^T$. Thus, the dynamic model of the crane is represented as

$$\begin{pmatrix} \dot{x}_1 \\ \dot{x}_2 \\ \dot{x}_3 \\ \dot{x}_4 \\ \dot{x}_5 \\ \dot{x}_6 \end{pmatrix} = \begin{pmatrix} x_2 \\ \frac{-M_{11}C_1 + M_{21}C_2 - M_{31}G_3}{detM} \\ x_4 \\ \frac{M_{12}C_1 - M_{22}C_2 + M_{32}G_3}{detM} \\ x_6 \\ \frac{-M_{13}C_1 + M_{23}C_2 - M_{33}G_3}{detM} \end{pmatrix} + \begin{pmatrix} 0 & 0 \\ \frac{M_{11}}{detM} & -\frac{M_{21}}{detM} \\ 0 & 0 \\ -\frac{M_{12}}{detM} & \frac{M_{22}}{detM} \\ 0 & 0 \\ \frac{M_{13}}{detM} & -\frac{M_{23}}{detM} \end{pmatrix} \begin{pmatrix} u_1 \\ u_2 \end{pmatrix} \tag{25}$$

or, equivalently, the crane's dynamics can be expressed in the nonlinear affine-in-the-input state-space form

$$\dot{x} = f(x) + g(x)u \tag{26}$$

$x \in R^{6\times 1}$, $f(x) \in R^{6\times 1}$, $g(x) \in R^{6\times 1}$, and $u \in R^{2\times 1}$. Nonlinear dynamics and underactuation make the solution of the associated control problem a nontrivial task.

2.2. Differential flatness properties of the 3-DOF cable-driven crane

It will be proven that the dynamic model of the two cable-driven 3-DOF robotic crane is differentially flat, with the flat outputs vector $Y = (x_R, y_R)^T$. It holds that

$$\begin{matrix} x_2 = \dot{x}_1 \Rightarrow x_2 = h_2(Y, \dot{Y}) \\ x_4 = \dot{x}_3 \Rightarrow x_4 = h_4(Y, \dot{Y}), \end{matrix} \tag{27}$$

which signifies that the state variables x_2, x_4 are differential functions of the flat outputs of the system. Besides, from the condition of Eq. (16) it holds that

$$\begin{matrix} -sin(\theta)\dot{x}_R + cos(\theta)\dot{y}_R = 0 \Rightarrow tan(\theta) = \frac{\dot{y}_R}{\dot{x}_R} \Rightarrow \theta = tan^{-1}(\frac{\dot{y}_R}{\dot{x}_R}) \\ \Rightarrow x_5 = \tan^{-1}(\frac{\dot{x}_3}{\dot{x}_1}) \Rightarrow x_5 = h_5(Y, \dot{Y}) \\ x_6 = \dot{x}_5 \Rightarrow x_6 = h_6(Y, \dot{Y}) \ , \end{matrix} \tag{28}$$

which signifies that the state variables x_5 and x_6 are also differential functions of the flat outputs of the system. Next, one uses Eq. (24), which in concise form is expressed as

$$\ddot{q} = \tilde{F}(q, \dot{q}) + \tilde{G}(q)u \ . \tag{29}$$

Using the Moore-Penrose matrix of $\tilde{G}(q)$ one obtains

$$u = [\tilde{G}^T(q)\tilde{G}(q)]^{-1}\tilde{G}^T(q)[\ddot{q} - \tilde{F}(q, \dot{q})], \tag{30}$$

where $q = [x_R, y_R, \theta]^T$. Thus, it is confirmed that the control inputs vector $u = [u_1, u_2]^T$ is a differential function of the flat outputs vector, or

$$u_1 = h_{u_1}(Y, \dot{Y}) \quad u_2 = h_{u_2}(Y, \dot{Y}) \ . \tag{31}$$

The proof of differential flatness properties for the robotic crane's model is an implicit proof of the system's controllability. Besides, it allows for treating the setpoints definition problem. One selects setpoints without constraints for state variables $x_1 = x_R$ and $x_3 = y_R$, which are associated with the flat outputs of the system. For the state variable θ, the setpoints should be chosen using the differential relation which connects this variable with the flat output $\theta_d = tan^{-1}(\frac{\dot{y}_R^d}{\dot{x}_R^d})$. At the steady state it holds that $\theta_d = 0$. The latter conclusion can be justified using Eq. (14) and the stabilization conditions $\dot{x}_R = 0$, $\ddot{x}_R = 0$, $\dot{y}_R = 0$, $\dot{y}_R = 0$, $\dot{\theta} = 0$, $\ddot{\theta} = 0$. Then, Eq. (14) gives $sin(\theta) = 0$, which also implies $\theta = 0$. Thus, at the steady-state of the two-cable 3-DOF crane, the setpoint for the swing angle θ of the payload is $\theta_d = 0$.

3. Approximate linearization of the two cable-driven 3-DOF robotic crane

The dynamic model of the two cable-driven 3-DOF crane undergoes approximate linearization with the use of first-order Taylor series expansion and through the computation of the associated Jacobian matrices. The linearization process takes place at each sampling instance around the temporary operating point (x^*, u^*), where x^* is the present value of the system's state vector and u^* is the last sampled value of the control inputs vector. The modelling error, which is due to the truncation of higher-order terms from the Taylor series expansion, is considered to be a perturbation, which is asymptotically compensated by the robustness of the control method.

The initial nonlinear state-space model of the crane being in the form $\dot{x} = f(x) + g(x)u$, after linearization turns into the form:

$$\dot{x} = Ax + Bu + \tilde{d} \tag{32}$$

where matrices A, B are the Jacobian matrices of the system:

$$\begin{aligned} A = \nabla_x[f(x) + g(x)u] \mid_{(x^*,u^*)} \Rightarrow & A = \nabla_x f(x) \mid_{(x^*,u^*)} + \\ & +\nabla_x g_1(x)u_1 \mid_{(x^*,u^*)} + \nabla_x g_2(x)u_2 \mid_{(x^*,u^*)} \end{aligned} \tag{33}$$

$$B = \nabla_u[f(x) + g(x)u] \mid_{(x^*,u^*)} \Rightarrow B = g(x) \mid_{(x^*,u^*)}, \tag{34}$$

where the cumulative vector od disturbances (x^*, u^*) comprises (i) modelling error due to truncation of higher-order terms from the Taylor series expansion, (ii) external disturbances, (iii) sensor measurement noise of any distribution. Because of linearizing at each sampling instance around the present position of the crane's state vector, the span of the Taylor series expansion is small and the modelling error is negligible. The procedure of computation of the Jacobian matrices of this robotic system is given in the Appendix.

Remark 1 *It is noted that the linearization approach, which has been followed for implementing the nonlinear optimal control scheme, results in a quite accurate model of the system's dynamics. Consider, for instance, the following* *affine-in-the-input state-space model*

$$\begin{aligned}
\dot{x} &= f(x) + g(x)u \Rightarrow \\
\dot{x} &= [f(x^*) + \nabla_x f(x) \mid_{x^*} (x - x^*)] + [g(x^*) + \nabla_x g(x) \mid_{x^*} (x - x^*)]u^* \\
&\qquad\qquad\qquad + g(x^*)u^* + g(x^*)(u - u^*) + \tilde{d}_1 \Rightarrow \\
\dot{x} &= [\nabla_x f(x) \mid_{x^*} + \nabla_x g(x) \mid_{x^*} u^*]x + g(x^*)u - [\nabla_x f(x) \mid_{x^*} \\
&\qquad + \nabla_x g(x) \mid_{x^*} u^*]x^* + f(x^*) + g(x^*)u^* + \tilde{d}_1
\end{aligned} \tag{35}$$

where $\tilde{d}_1$ is the modelling error, due to truncation of higher order terms in the Taylor series expansion of $f(x)$ and $g(x)$. Next, by defining $A = [\nabla_x f(x) \mid_{x^*} + \nabla_x g(x) \mid_{x^*} u^*]$, $B = g(x^*)$, one obtains

$$\dot{x} = Ax + Bu - Ax^* + f(x^*) + g(x^*)u^* + \tilde{d}_1 \ . \tag{36}$$

Moreover, by denoting $\tilde{d} = -Ax^* + f(x^*) + g(x^*)u^* + \tilde{d}_1$ about the cumulative modelling error term in the Taylor series expansion procedure one has

$$\dot{x} = Ax + Bu + \tilde{d} \tag{37}$$

which is the approximately linearized model of the dynamics of the system of Eq. (32). The term $f(x^*) + g(x^*)u^*$ is the derivative of the state vector at (x^*, u^*), which is almost annihilated by $-Ax^*$.

4. Design of an H-infinity nonlinear feedback controller

4.1. Equivalent linearized dynamics of the two cable-driven 3-DOF robotic crane

After linearization around its current operating point, the dynamic model for the two cable-driven 3-DOF robotic crane is written as

$$\dot{x} = Ax + Bu + d_1 \ . \tag{38}$$

Parameter d_1 stands for the linearization error in the two cable-driven 3-DOF robotic crane's model that was given previously in Eq. (38). The reference setpoints for the state vector of the aforementioned dynamic model are denoted by $\mathbf{x_d} = [x_1^d, \cdots, x_6^d]$. Tracking of this trajectory is achieved after applying the control input u^*. At every time instant, the control input u^* is assumed to differ from the control input u, appearing in Eq. (38), by a value equal to Δu, that is, $u^* = u + \Delta u$

$$\dot{x}_d = Ax_d + Bu^* + d_2 \ . \tag{39}$$

The dynamics of the controlled system, described in Eq. (38), can be also written down as

$$\dot{x} = Ax + Bu + Bu^* - Bu^* + d_1 \tag{40}$$

and by denoting $d_3 = -Bu^* + d_1$ as an aggregate disturbance term, one obtains

$$\dot{x} = Ax + Bu + Bu^* + d_3 \ . \tag{41}$$

By subtracting Eq. (39) from Eq. (41), one gets

$$\dot{x} - \dot{x}_d = A(x - x_d) + Bu + d_3 - d_2 \ . \tag{42}$$

Upon denoting the tracking error as $e = x - x_d$ and the aggregate disturbance term as $L\tilde{d} = d_3 - d_2$, the tracking error dynamics becomes

$$\dot{e} = Ae + Bu + L\tilde{d}, \tag{43}$$

where L is a disturbance inputs gain matrix. The above linearized form of the two cable-driven 3-DOF robotic crane's model can be efficiently controlled after applying an H-infinity feedback control scheme.

4.2. The nonlinear H-infinity control

The initial nonlinear model of the two cable-driven 3-DOF robotic crane is in the form

$$\dot{x} = f(x, u) \ \ x \in R^n, \ u \in R^m. \tag{44}$$

Linearization of the model of the two cable-driven 3-DOF robotic crane is performed at each iteration of the control algorithm around its present operating point $(x^*, u^*) = (x(t), u(t - T_s))$. The linearized equivalent of the system is described by

$$\dot{x} = Ax + Bu + L\tilde{d} \ \ x \in R^n, \ u \in R^m, \ \tilde{d} \in R^q \tag{45}$$

where matrices A and B are obtained from the computation of the previously defined Jacobians and vector $\tilde{d}$ denotes disturbance terms due to linearization errors, while L is a disturbance inputs gain matrix. The problem of disturbance rejection for the linearized model that is described by

$$\begin{aligned} \dot{x} &= Ax + Bu + L\tilde{d} \\ y &= Cx \end{aligned} \tag{46}$$

where $x \in R^n$, $u \in R^m$, $\tilde{d} \in R^q$ and $y \in R^p$, cannot be handled efficiently if the classical LQR control scheme is applied. This is because of the existence of the perturbation term $\tilde{d}$. The disturbance term $\tilde{d}$, apart from modeling (parametric) uncertainty and external perturbations, can also represent noise terms of any distribution.

In the H_∞ control approach, a feedback control scheme is designed for trajectory tracking by the system's state vector and simultaneous disturbance rejection, considering that the disturbance affects the system in the worst possible manner. The disturbance effects are incorporated in the following quadratic cost function:

$$J(t) = \frac{1}{2}\int_0^T [y^T(t)y(t) + ru^T(t)u(t) - \rho^2 \tilde{d}^T(t)\tilde{d}(t)]dt, \quad r, \rho > 0 \ . \tag{47}$$

The significance of the negative sign in the cost function term that is associated with the perturbation variable $\tilde{d}(t)$ is that the disturbance tries to maximize the cost function $J(t)$, while the control signal $u(t)$ tries to minimize it. The physical meaning of the relation given above is that the control signal and the disturbances compete with each other within a min-max differential game. This problem of min-max optimization can be expressed as $min_u max_{\tilde{d}} J(u, \tilde{d})$.

The objective of the optimization procedure is to compute a control signal $u(t)$, which can compensate for the worst possible disturbance, that is externally imposed on the two cable-driven 3-DOF robotic crane. However, the solution to the min-max optimization problem is directly related to the value of parameter ρ. This means that there is an upper bound in the disturbance magnitude that can be annihilated by the control signal.

4.3. Computation of the feedback control gains

For the linearized system, given by Eq. (46), the cost function of Eq. (47) is defined, where coefficient r determines the penalization of the control input and weight coefficient ρ determines the reward of the disturbances' effects. It is assumed that (i) the energy that is transferred from the disturbance signal $\tilde{d}(t)$ is bounded, that is, $\int_0^\infty \tilde{d}^T(t)\tilde{d}(t)dt < \infty$, (ii) matrices $[A, B]$ and $[A, L]$ are stabilizable, (iii) matrix $[A, C]$ is detectable. In the case of a tracking problem the optimal feedback control law is given by

$$u(t) = -Ke(t) \tag{48}$$

with $e = x - x_d$ being the tracking error, and $K = \frac{1}{r}B^T P$, where P is a positive definite symmetric matrix. As it will be proven in Section 5, matrix P is obtained from the solution of the Riccati equation

$$A^T P + PA + Q - P(\frac{2}{r}BB^T - \frac{1}{\rho^2}LL^T)P = 0 \tag{49}$$

where Q is a positive semi-definite symmetric matrix. The worst-case disturbance is given by

$$\tilde{d}(t) = \frac{1}{\rho^2} L^T P e(t) \ . \tag{50}$$

The solution of the H-infinity feedback control problem for the two cable-driven 3-DOF robotic crane and the computation of the worst case disturbance that the related controller can sustain, comes from the superposition of Bellman's optimality principle when considering that the two cable-driven 3-DOF robotic crane is affected by two separate inputs (i) the control input u, and (ii), the cumulative disturbance input $\tilde{d}(t)$. Solving the optimal control problem for u, that is, for the minimum variation (optimal) control input that achieves elimination of the state vector's tracking error, gives $u = -\frac{1}{r} B^T P e$. Equivalently, solving the optimal control problem for $\tilde{d}$, that is, for the worst-case disturbance that the control loop can sustain, gives $\tilde{d} = \frac{1}{\rho^2} L^T P e$.

The diagram of the considered control loop for the two cable-driven 3-DOF robotic crane is presented in Fig. 2.

Figure 2 gives also a block diagram for the nonlinear optimal control scheme. The implementation stages of the control method can be formulated as follows:

(1) at each sampling instance there is linearization of the state-space model of the 3-DOF two-cable driven robotic crane around a time-varying operating point, which is defined by the present value of the system's state vector and by the last sampled value of the control inputs vector. The linearization is performed through first-order Taylor series expansion and the computation of the associated Jacobian matrices,

(2) for the approximately linearized model of the 3-DOF two-cable driven robotic crane an H-infinity feedback controller is designed. To compute the controller's feedback gains an algebraic Riccati equation is also repetitively solved at each time-step of the control algorithm. Main parameters of this Riccati equation are the gains r and ρ, as well as the gain matrices Q and L,

(3) the computed optimal control inputs are applied directly to the initial nonlinear state-space model of the system.

The global stability of the control method and the elimination of the state vector's tracking error are confirmed through Lyapunov analysis. The computational effort for the implementation of this control method is moderate and the solution of the method's Riccati equation is achieved in a time interval, which is smaller than the sampling period.

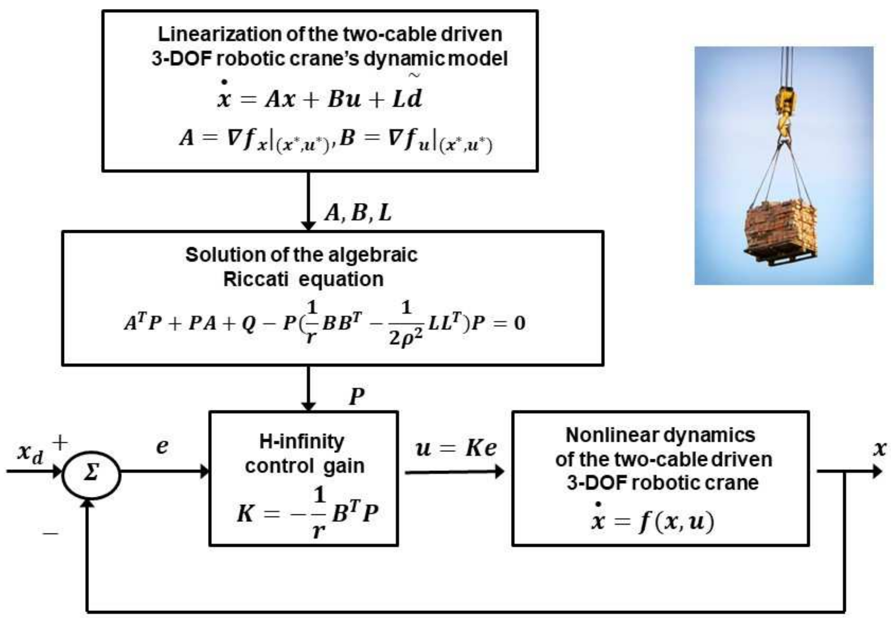

Figure 2. Control scheme and implementation stages for the two cable-driven 3-DOF robotic crane

5. Lyapunov stability analysis

5.1. Stability proof

Through Lyapunov stability analysis it will be shown that the proposed nonlinear control scheme assures H_∞ tracking performance for the two cable-driven 3-DOF robotic crane, and that in the case of bounded disturbance terms asymptotic convergence to the reference setpoints is achieved. The tracking error dynamics for the two cable-driven 3-DOF robotic crane is expressed in the form

$$\dot{e} = Ae + Bu + L\tilde{d}, \tag{51}$$

where in the two cable-driven 3-DOF robotic crane's case $L{\in}R^{6\times 6}$ is the disturbance inputs gain matrix. Variable $\tilde{d}$ denotes model uncertainties and external disturbances of the two cable-driven 3-DOF robotic crane's model.

The following Lyapunov equation is considered

$$V = \tfrac{1}{2}e^T Pe \tag{52}$$

where $e = x - x_d$ is the tracking error. By differentiating with respect to time one obtains

$$\begin{aligned} \dot{V} &= \tfrac{1}{2}\dot{e}^T Pe + \tfrac{1}{2}e^T P\dot{e} \Rightarrow \\ \dot{V} &= \tfrac{1}{2}[Ae + Bu + L\tilde{d}]^T Pe + \tfrac{1}{2}e^T P[Ae + Bu + L\tilde{d}] \end{aligned} \tag{53}$$

$$\begin{aligned} \dot{V} = \, & \tfrac{1}{2}[e^T A^T + u^T B^T + \tilde{d}^T L^T]Pe + \\ & +\tfrac{1}{2}e^T P[Ae + Bu + L\tilde{d}] \end{aligned} \tag{54}$$

$$\begin{aligned} \dot{V} = \, & \tfrac{1}{2}e^T A^T Pe + \tfrac{1}{2}u^T B^T Pe + \tfrac{1}{2}\tilde{d}^T L^T Pe + \\ & \tfrac{1}{2}e^T PAe + \tfrac{1}{2}e^T PBu + \tfrac{1}{2}e^T PL\tilde{d} \ . \end{aligned} \tag{55}$$

The previous equation is rewritten as

$$\begin{aligned} \dot{V} = \, & \tfrac{1}{2}e^T (A^T P + PA)e + (\tfrac{1}{2}u^T B^T Pe + \tfrac{1}{2}e^T PBu) + \\ & +(\tfrac{1}{2}\tilde{d}^T L^T Pe + \tfrac{1}{2}e^T PL\tilde{d}). \end{aligned} \tag{56}$$

Assumption 1 *For given positive definite matrix Q and coefficients r and ρ there exists a positive definite matrix P, which is the solution of the following matrix equation*

$$A^T P + PA = -Q + P(\tfrac{2}{r}BB^T - \tfrac{1}{\rho^2}LL^T)P \ . \tag{57}$$

Moreover, the following feedback control law is applied to the system

$$u = -\tfrac{1}{r}B^T Pe \ . \tag{58}$$

By substituting Eq. (57) and Eq. (58) one obtains

$$\begin{aligned}\dot{V} = &\tfrac{1}{2}e^T[-Q+P(\tfrac{2}{r}BB^T-\tfrac{1}{\rho^2}LL^T)P]e+\\ &+e^TPB(-\tfrac{1}{r}B^TPe)+e^TPL\tilde{d}\Rightarrow\end{aligned} \tag{59}$$

$$\begin{aligned}\dot{V} = &-\tfrac{1}{2}e^TQe+\tfrac{1}{r}e^TPBB^TPe-\tfrac{1}{2\rho^2}e^TPLL^TPe\\ &-\tfrac{1}{r}e^TPBB^TPe+e^TPL\tilde{d}\end{aligned} \tag{60}$$

which, after intermediate operations, gives

$$\dot{V} = -\tfrac{1}{2}e^TQe-\tfrac{1}{2\rho^2}e^TPLL^TPe+e^TPL\tilde{d} \tag{61}$$

or, equivalently

$$\begin{aligned}\dot{V} = &-\tfrac{1}{2}e^TQe-\tfrac{1}{2\rho^2}e^TPLL^TPe+\\ &+\tfrac{1}{2}e^TPL\tilde{d}+\tfrac{1}{2}\tilde{d}^TL^TPe\ .\end{aligned} \tag{62}$$

Lemma 1 *The following inequality holds*

$$\tfrac{1}{2}e^TPL\tilde{d}+\tfrac{1}{2}\tilde{d}L^TPe-\tfrac{1}{2\rho^2}e^TPLL^TPe\leq\tfrac{1}{2}\rho^2\tilde{d}^T\tilde{d}. \tag{63}$$

Proof The binomial $(\rho a-\frac{1}{\rho}b)^2$ is considered. By expanding the left part of the above inequality, one gets

$$\begin{aligned}&\rho^2a^2+\tfrac{1}{\rho^2}b^2-2ab\geq 0\Rightarrow\tfrac{1}{2}\rho^2a^2+\tfrac{1}{2\rho^2}b^2-ab\geq 0\Rightarrow\\ &ab-\tfrac{1}{2\rho^2}b^2\leq\tfrac{1}{2}\rho^2a^2\Rightarrow\tfrac{1}{2}ab+\tfrac{1}{2}ab-\tfrac{1}{2\rho^2}b^2\leq\tfrac{1}{2}\rho^2a^2\ .\end{aligned} \tag{64}$$

The following substitutions are carried out: $a=\tilde{d}$ and $b=e^TPL$ and the previous relation becomes

$$\tfrac{1}{2}\tilde{d}^TL^TPe+\tfrac{1}{2}e^TPL\tilde{d}-\tfrac{1}{2\rho^2}e^TPLL^TPe\leq\tfrac{1}{2}\rho^2\tilde{d}^T\tilde{d}\ . \tag{65}$$

Eq. (65) is substituted in Eq. (62) and the inequality is enforced, thus giving

$$\dot{V}\leq-\tfrac{1}{2}e^TQe+\tfrac{1}{2}\rho^2\tilde{d}^T\tilde{d}\ . \tag{66}$$

Eq. (66) shows that the H_∞ tracking performance criterion is satisfied. The integration of $\dot{V}$ from 0 to T gives

$$\begin{aligned}&\int_0^T\dot{V}(t)dt\leq-\tfrac{1}{2}\int_0^T||e||_Q^2dt+\tfrac{1}{2}\rho^2\int_0^T||\tilde{d}||^2dt\Rightarrow\\ &2V(T)+\int_0^T||e||_Q^2dt\leq 2V(0)+\rho^2\int_0^T||\tilde{d}||^2dt\ .\end{aligned} \tag{67}$$

Moreover, if there exists a positive constant $M_d>0$ such that

$$\int_0^\infty||\tilde{d}||^2dt\leq M_d \tag{68}$$

then one gets

$$\int_0^\infty ||e||_Q^2 dt \leq 2V(0) + \rho^2 M_d \ . \tag{69}$$

Thus, the integral $\int_0^\infty ||e||_Q^2 dt$ is bounded. Moreover, $V(T)$ is bounded and from the definition of the Lyapunov function V in Eq. (52) it becomes clear that $e(t)$ will be also bounded, since $e(t) \ \in \ \Omega_e = \{e|e^T Q e \leq 2V(0) + \rho^2 M_d\}$. According to the above, and with the use of Barbalat's Lemma one obtains $\lim_{t\to\infty} e(t) = 0$.

After following the stages of the stability proof one arrives at Eq. (66) which shows that the H-infinity tracking performance criterion holds. By selecting the attenuation coefficient ρ to be sufficiently small and, in particular, to satisfy $\rho^2 \ < \ ||e||_Q^2/||\tilde{d}||^2$, one has that the first derivative of the Lyapunov function is upper bounded by 0. This condition holds at each sampling instance and, consequently, global stability for the control loop can be concluded. ∎

5.2. Robust state estimation with the use of the H_∞ Kalman filter

The control loop has to be implemented with the use of information provided by a small number of sensors and by processing only a small number of state variables. To reconstruct the missing information about the state vector of the two cable-driven 3-DOF robotic crane it is proposed to use a filtering scheme and, on its basis, to apply the state estimation-based control (Rigatos, 2016; Rigatos, Abbaszadeh and Siano, 2022). By denoting as $A(k)$, $B(k)$ and $C(k)$ the discrete-time equivalents of matrices, respectively, A, B and C of the linearized state-space model of the system, the recursion of the H_∞ Kalman Filter for the model of the two cable-driven 3-DOF robotic crane, can be formulated in terms of a *measurement update* and a *time update* part

Measurement update:

$$\begin{array}{l} D(k) = [I - \bar{\theta} W(k) P^-(k) + C^T(k) R(k)^{-1} C(k) P^-(k)]^{-1} \\ K(k) = P^-(k) D(k) C^T(k) R(k)^{-1} \\ \hat{x}(k) = \hat{x}^-(k) + K(k)[y(k) - C\hat{x}^-(k)] \ . \end{array} \tag{70}$$

Time update:

$$\begin{array}{l} \hat{x}^-(k+1) = A(k)x(k) + B(k)u(k) \\ P^-(k+1) = A(k)P^-(k)D(k)A^T(k) + Q(k) \ , \end{array} \tag{71}$$

where it is assumed that parameter θ is sufficiently small to assure that the covariance matrix

$$P^-(k)^{-1} - \bar{\theta} W(k) + C^T(k) R(k)^{-1} C(k)$$

will be positive definite. When $\theta = 0$, the H_∞ Kalman Filter becomes equivalent to the standard Kalman Filter. One can measure only a part of the state vector of the crane, for instance, the state variables x_1, x_3, x_5, and can estimate through filtering the rest of the state vector elements (velocity variables x_2, x_4, x_6). Moreover, the proposed Kalman filtering method can be used for sensor fusion purposes.

6. Simulation tests

The global stability properties of the control method and the elimination of the state vector's tracking error, which were previously proven through Lyapunov analysis, are further confirmed through simulation experiments. Indicative values for the parameters of the crane's model have been: $M = 1.0\,kg$, $m = 1.0\,kg$, $L_3 = 0.5\,m$ and $g = 10\,m/sec^2$. The sampling period was $T_s = 0.01$ *sec*. To implement the control method one had to solve at each sampling instance the algebraic Riccati equation of Eq. (57). The obtained results are shown in a series of illustrations, from Fig. 3 to Fig. 18. In the related diagrams, the real values of the state vector elements are printed in blue color, the reference setpoints are plotted in red color, while the estimated values of the state variables are depicted in green color.

It can be noticed that in all test cases the control method applied achieved fast and accurate tracking of reference setpoints by the state variables of the crane under minimal variations of the control inputs. By keeping small the amplitude of the control signal, the nonlinear optimal control method achieves also the minimization of the dispersion of energy by the actuators (motors) of this robotic system. The transient performance of the control method depends on the selection of values for the main parameters r, ρ, Q of the method's Riccati equation. For relatively small values of r, the state vector's tracking error is eliminated. For relatively large values of the diagonal elements of matrix Q, the speed of convergence to setpoints is increased. Finally, the smallest value of ρ, for which one obtains a valid solution of the method's Riccati equation, is the one that provides the control loop with maximum robustness.

Comparing to other nonlinear control schemes that one could have considered for the dynamic model of the two cable-driven 3-DOF robotic crane, the following can be stated:

(i) unlike global linearization-based control schemes, such as Lie-algebra-based control and flatness-based control with transformation into canonical forms, the nonlinear optimal control method does nor need complicated changes of state variables (diffeomorphisms) and state-space model transformations. The control inputs are computed for the initial nonlinear state-space model of the system without the need for inverse transformations and without coming against the risk of singularities (non-invertibility);

(ii) unlike Nonlinear Model Predictive Control (NMPC), the global stability properties are proven and the convergence of the iterative search for the optimum of the new nonlinear optimal control method does not depend on initialization and ad-hoc selection of the controller's parameters;

(iii) unlike sliding-mode control and backstepping control, the application of the new nonlinear optimal control method does not have as a prerequisite the dynamic model of the system to be found in a specific state-space form (for instance, the canonical form, the input-output linearized form, or the strict-feedback form). For example, it is known that unless a nonlinear system is established in the input-output linearized form, there is no systematic manner for defining a sliding surface and a sliding-mode controller about it. Additionally, unless a nonlinear system is found in the strict-feedback (triangular) form, the application of the backstepping control method is not a straightforward procedure;

(iv) unlike PID control, the new nonlinear optimal control method is of proven global stability and the selection of the controller's gains is not based on heuristics. The nonlinear optimal control loop remains reliable at changes of operating points and time-varying setpoints, and

(v) unlike multiple local model-based feedback control, the nonlinear optimal control method uses only one linearization point and needs the solution of only one Riccati equation, therefore it is computationally more efficient.

To elaborate on nonlinear optimal control for the 3-DOF two-cable driven robotic crane the following tables are given:

(i) Table I, providing the results concerning the accuracy of tracking of setpoints by the state variables of the 3-DOF two-cable driven robotic crane under an exact dynamic model,

(ii) Table II, providing the results, concerning the accuracy of tracking of setpoints by the state variables of the 3-DOF two-cable driven robotic crane under a model that is subject to disturbances (for instance, change of $\Delta\alpha\%$ in the mass M of the cart),

(iii) Table III, providing the results, concerning the accuracy of state estimation for the 3-DOF two-cable driven robotic crane provided by the H-infinity Kalman Filter, and

(iv) Table IV, providing the results concerning the convergence times to setpoints of the state variables of the 3-DOF two-cable driven robotic crane.

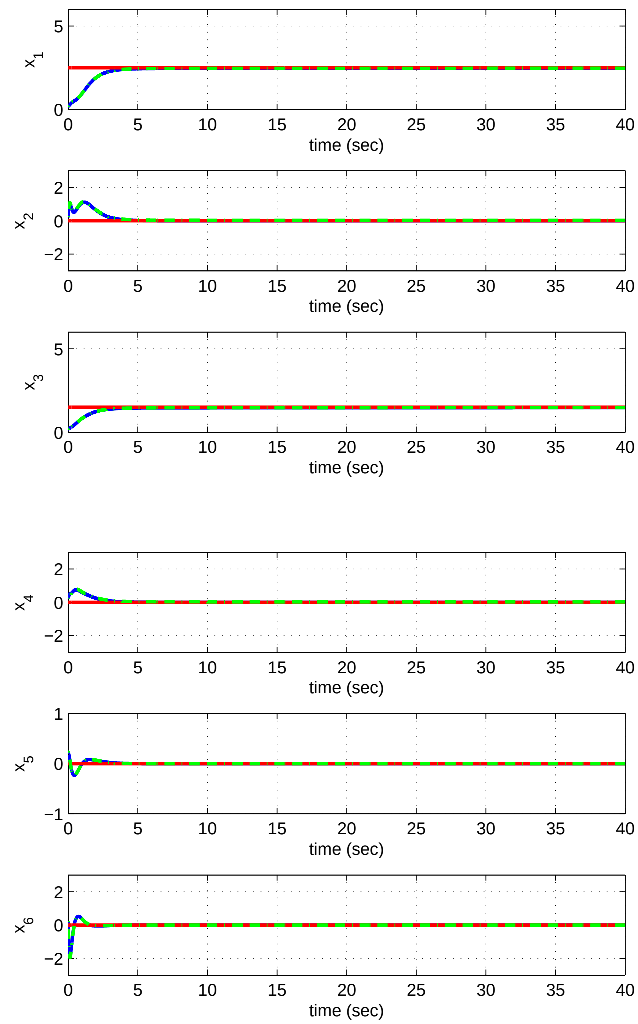

Figure 3. Tracking of setpoint 1 by the two cable-driven 3-DOF robotic crane with nonlinear optimal control: (top) tracking of setpoints (red line) by the state variables of the crane x_1 to x_3 (blue line) and estimates provided by the H-infinity Kalman Filter, (bottom) tracking of setpoints (red line) by the state variables of the crane x_4 to x_6 (blue line) and estimates provided by the H-infinity Kalman Filter

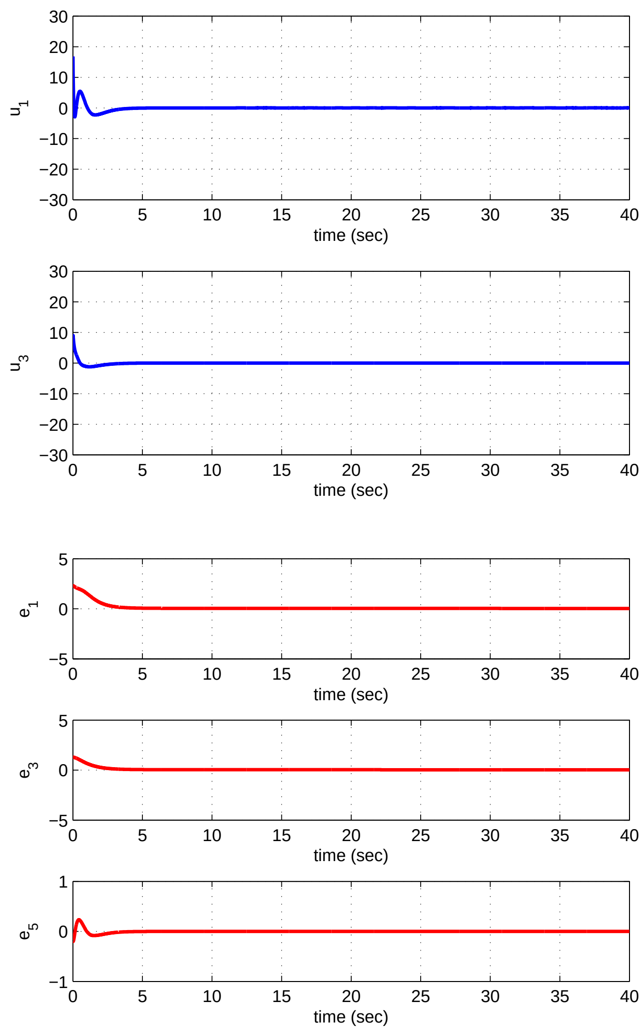

Figure 4. Tracking of setpoint 1 by the two cable-driven 3-DOF robotic crane with nonlinear optimal control: (top) variations of the control inputs of the gantry crane u_1 and u_2 (blue line), (bottom) convergence to 0 of the tracking error variables e_1, e_3 and e_5 associated with state variables $x_1 = x_R$, $x_3 = y_R$ and $x_5 = \theta$

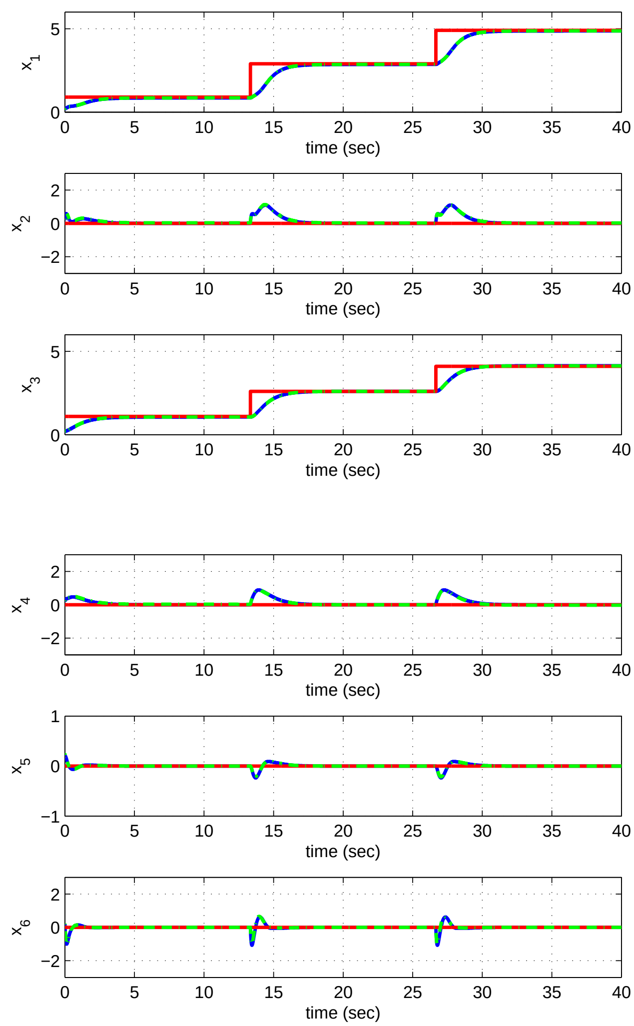

Figure 5. Tracking of setpoint 2 by the two cable-driven 3-DOF robotic crane with nonlinear optimal control: (top) tracking of setpoints (red line) by the state variables of the crane x_1 to x_3 (blue line) and estimates provided by the H-infinity Kalman Filter, (bottom) tracking of setpoints (red line) by the state variables of the crane x_4 to x_6 (blue line) and estimates provided by the H-infinity Kalman Filter

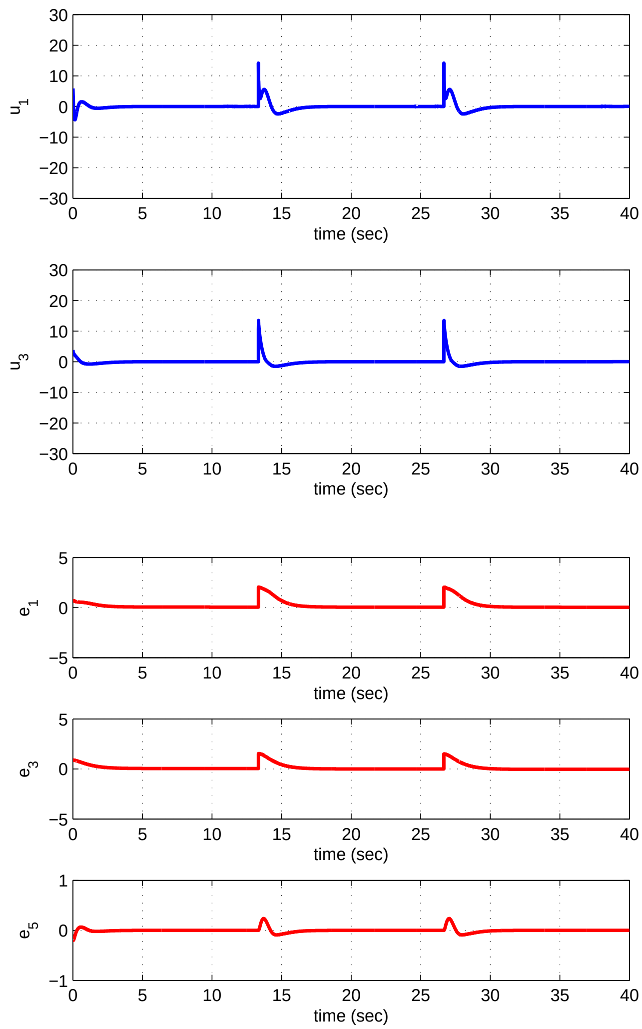

Figure 6. Tracking of setpoint 2 by the two cable-driven 3-DOF robotic crane with nonlinear optimal control: (top) variations of the control inputs of the gantry crane u_1 and u_2 (blue line), (bottom) convergence to 0 of the tracking error variables e_1, e_3 and e_5 associated with state variables $x_1 = x_R$, $x_3 = y_R$ and $x_5 = \theta$

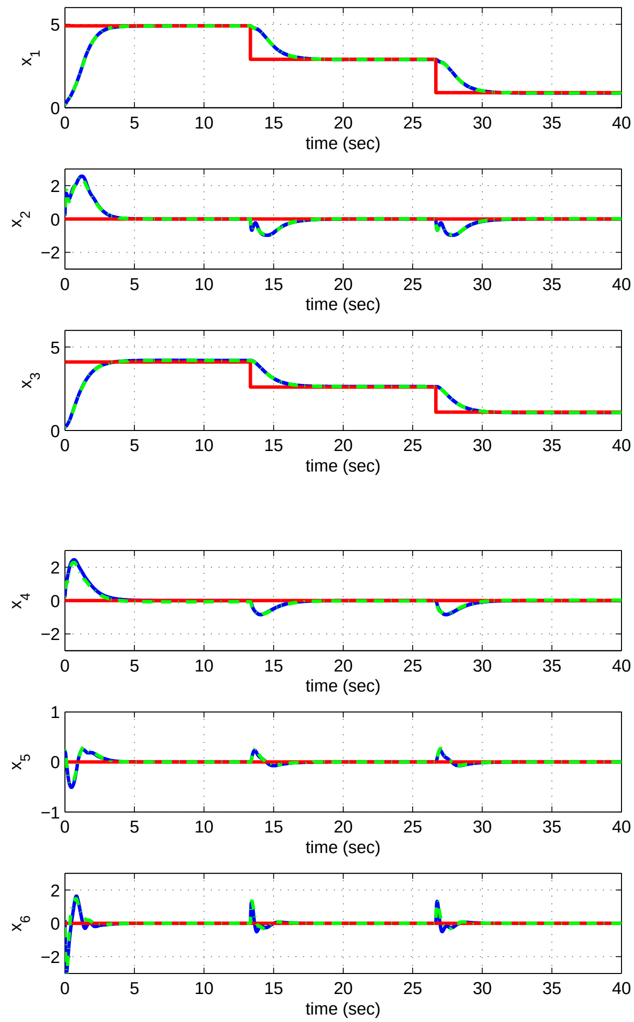

Figure 7. Tracking of setpoint 3 by the two cable-driven 3-DOF robotic crane with nonlinear optimal control: (top) tracking of setpoints (red line) by the state variables of the crane x_1 to x_3 (blue line) and estimates provided by the H-infinity Kalman Filter, (bottom) tracking of setpoints (red line) by the state variables of the crane x_4 to x_6 (blue line) and estimates provided by the H-infinity Kalman Filter

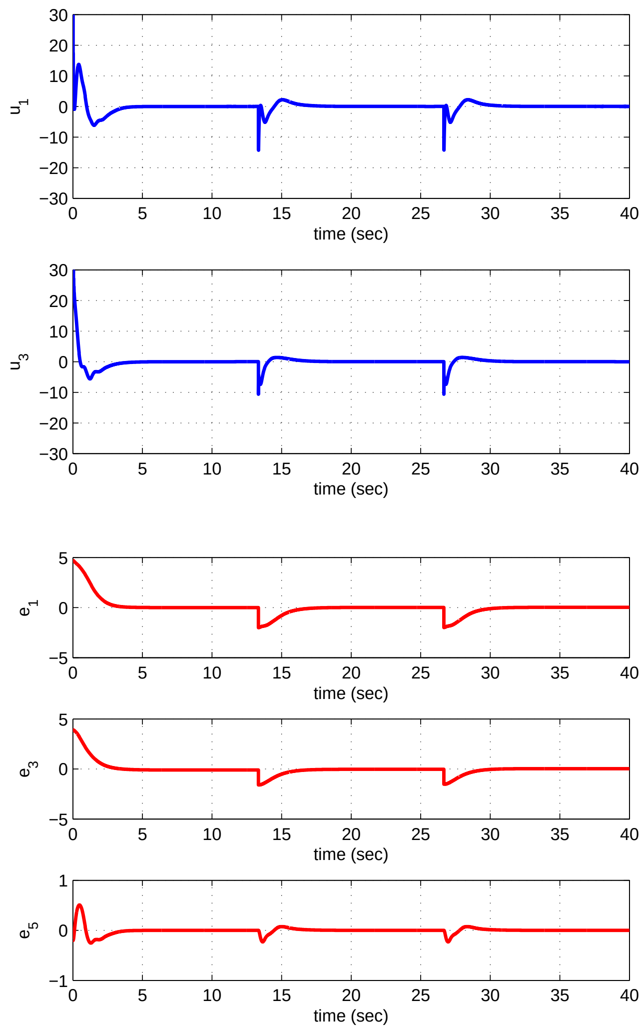

Figure 8. Tracking of setpoint 3 by the two cable-driven 3-DOF robotic crane with nonlinear optimal control: (top) variations of the control inputs of the gantry crane u_1 and u_2 (blue line), (bottom) convergence to 0 of the tracking error variables e_1, e_3 and e_5 associated with state variables $x_1 = x_R$, $x_3 = y_R$ and $x_5 = \theta$

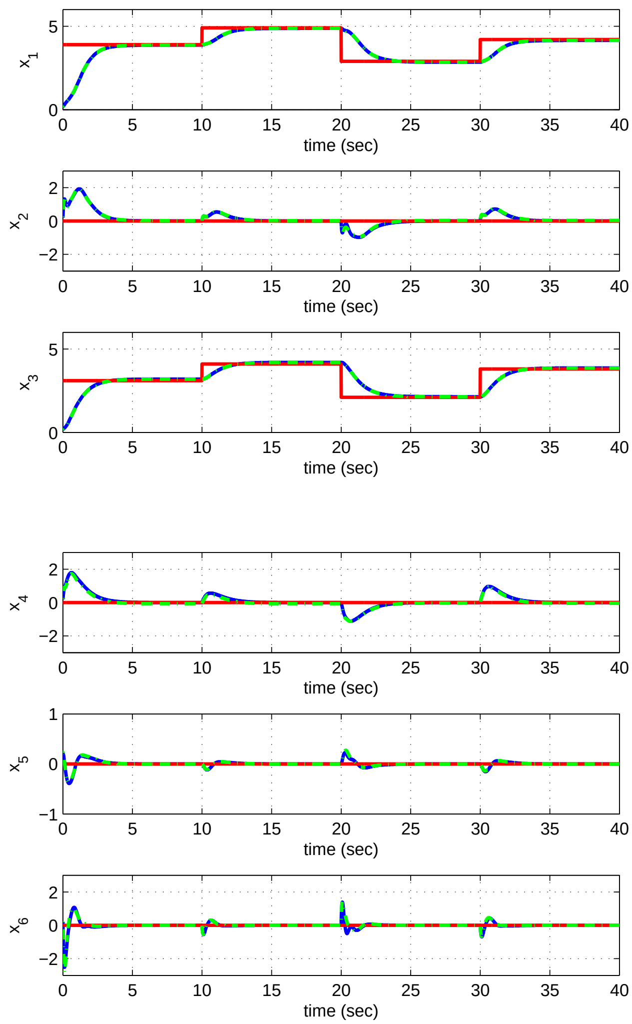

Figure 9. Tracking of setpoint 4 by the two cable-driven 3-DOF robotic crane with nonlinear optimal control: (top) tracking of setpoints (red line) by the state variables of the crane x_1 to x_3 (blue line) and estimates provided by the H-infinity Kalman Filter, (bottom) tracking of setpoints (red line) by the state variables of the crane x_4 to x_6 (blue line) and estimates provided by the H-infinity Kalman Filter

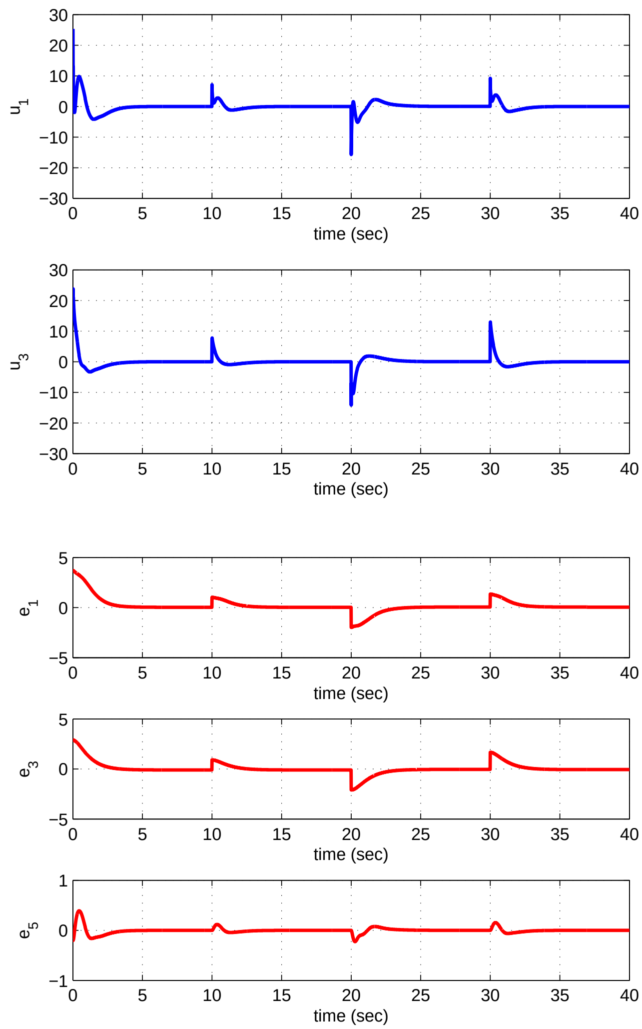

Figure 10. Tracking of setpoint 4 by the two cable-driven 3-DOF robotic crane with nonlinear optimal control: (top) variations of the control inputs of the gantry crane u_1 and u_2 (blue line), (bottom) convergence to 0 of the tracking error variables e_1, e_3 and e_5 associated with state variables $x_1 = x_R$, $x_3 = y_R$ and $x_5 = \theta$

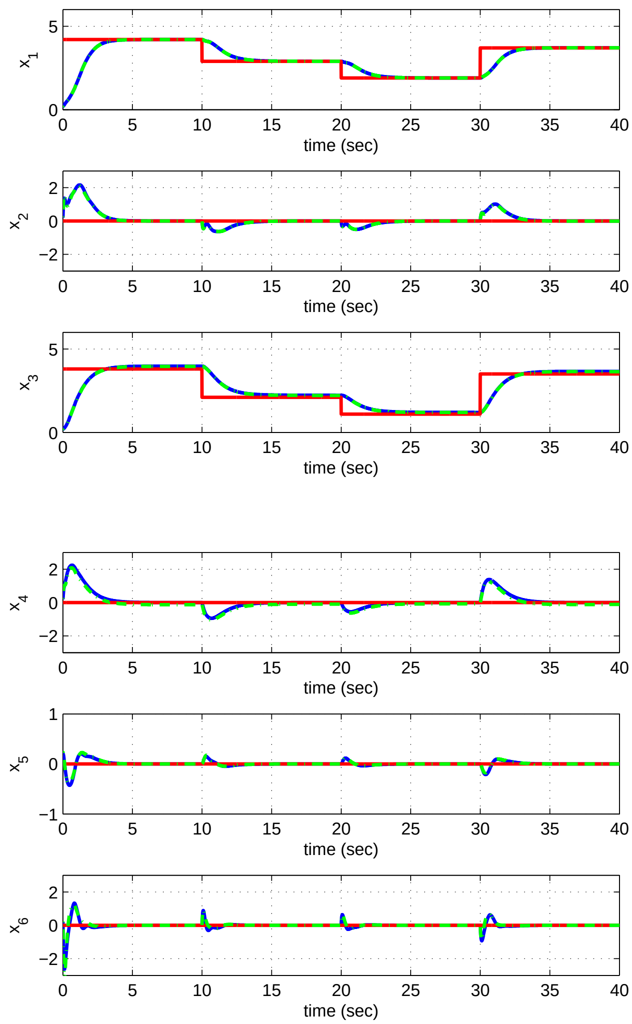

Figure 11. Tracking of setpoint 5 by the two cable-driven 3-DOF robotic crane with nonlinear optimal control: (top) tracking of setpoints (red line) by the state variables of the crane x_1 to x_3 (blue line) and estimates provided by the H-infinity Kalman Filter, (bottom) tracking of setpoints (red line) by the state variables of the crane x_4 to x_6 (blue line) and estimates provided by the H-infinity Kalman Filter

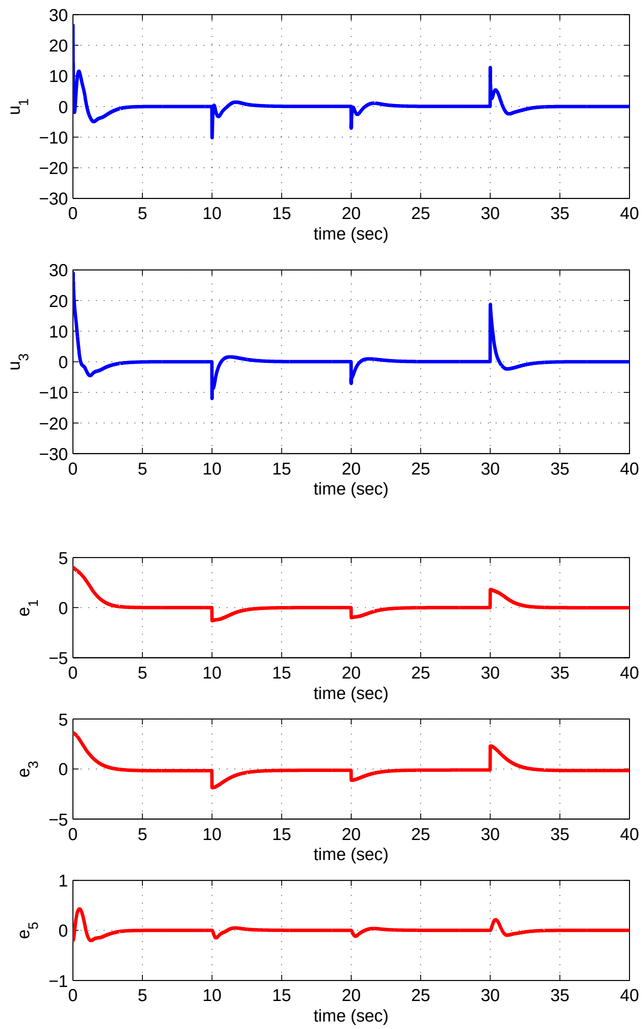

Figure 12. Tracking of setpoint 5 by the two cable-driven 3-DOF robotic crane with nonlinear optimal control: (top) variations of the control inputs of the gantry crane u_1 and u_2 (blue line), (bottom) convergence to 0 of the tracking error variables e_1, e_3 and e_5 associated with state variables $x_1 = x_R$, $x_3 = y_R$ and $x_5 = \theta$

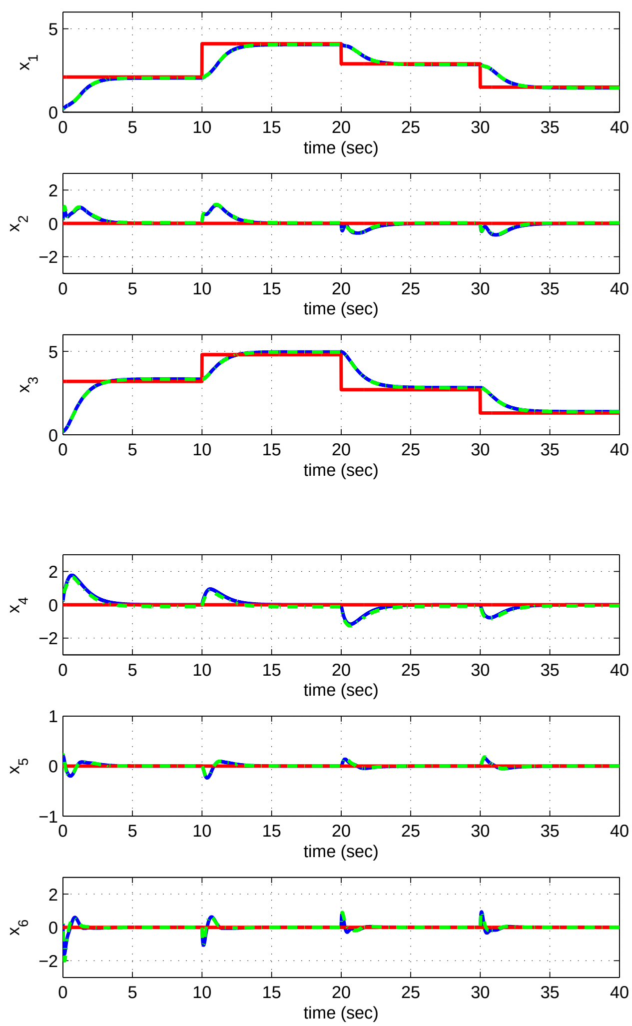

Figure 13. Tracking of setpoint 6 by the two cable-driven 3-DOF robotic crane with nonlinear optimal control: (top) tracking of setpoints (red line) by the state variables of the crane x_1 to x_3 (blue line) and estimates provided by the H-infinity Kalman Filter, (bottom) tracking of setpoints (red line) by the state variables of the crane x_4 to x_6 (blue line) and estimates provided by the H-infinity Kalman Filter

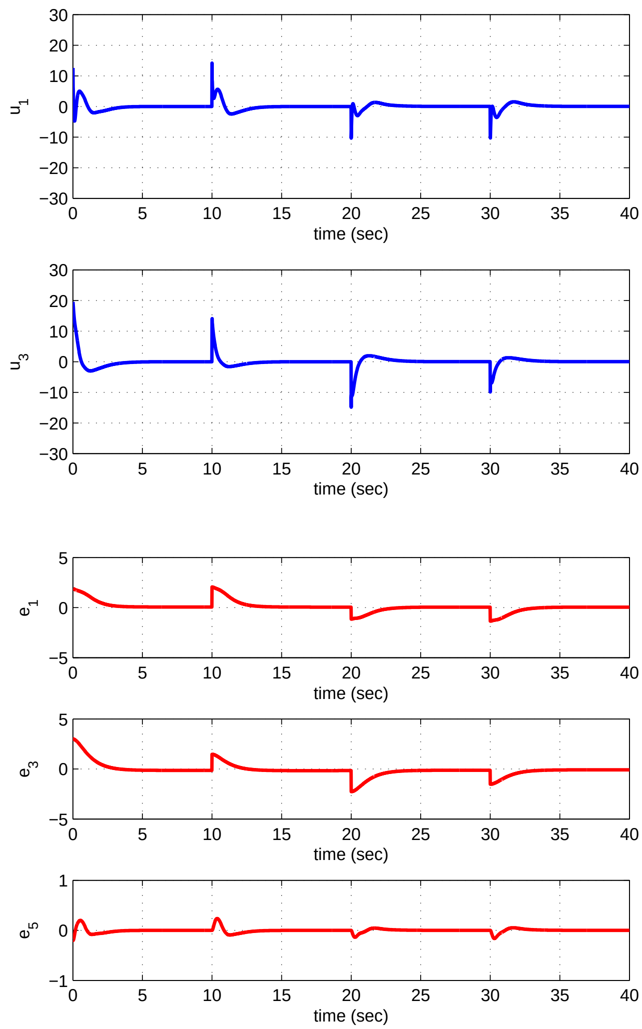

Figure 14. Tracking of setpoint 6 by the two cable-driven 3-DOF robotic crane with nonlinear optimal control: (top) variations of the control inputs of the gantry crane u_1 and u_2 (blue line), (bottom) convergence to 0 of the tracking error variables e_1, e_3 and e_5 associated with state variables $x_1 = x_R$, $x_3 = y_R$ and $x_5 = \theta$

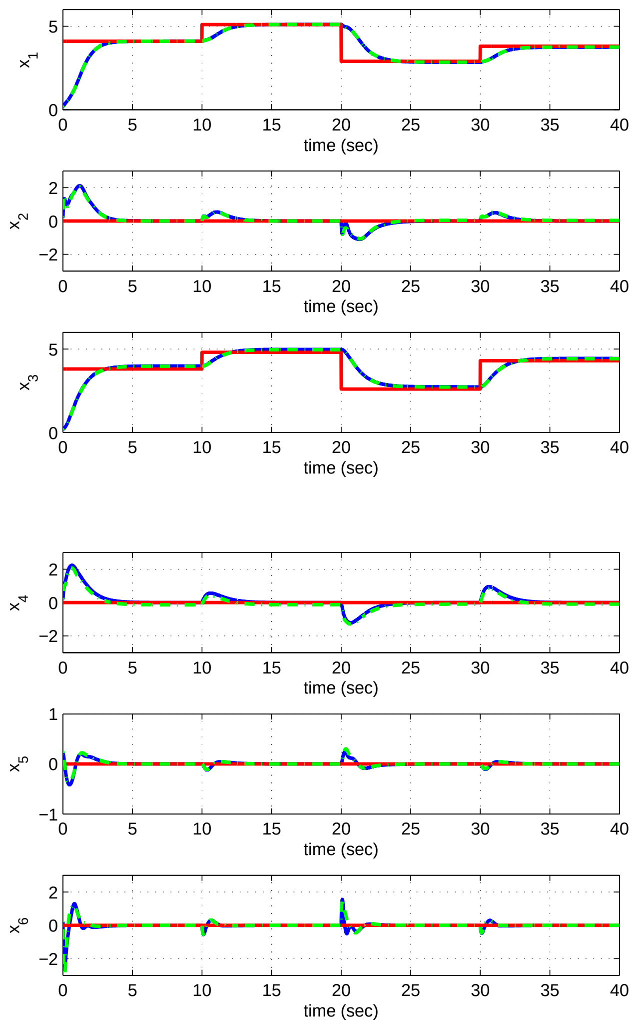

Figure 15. Tracking of setpoint 7 by the two cable-driven 3-DOF robotic crane with nonlinear optimal control: (top) tracking of setpoints (red line) by the state variables of the crane x_1 to x_3 (blue line) and estimates provided by the H-infinity Kalman Filter, (bottom) tracking of setpoints (red line) by the state variables of the crane x_4 to x_6 (blue line) and estimates provided by the H-infinity Kalman Filter

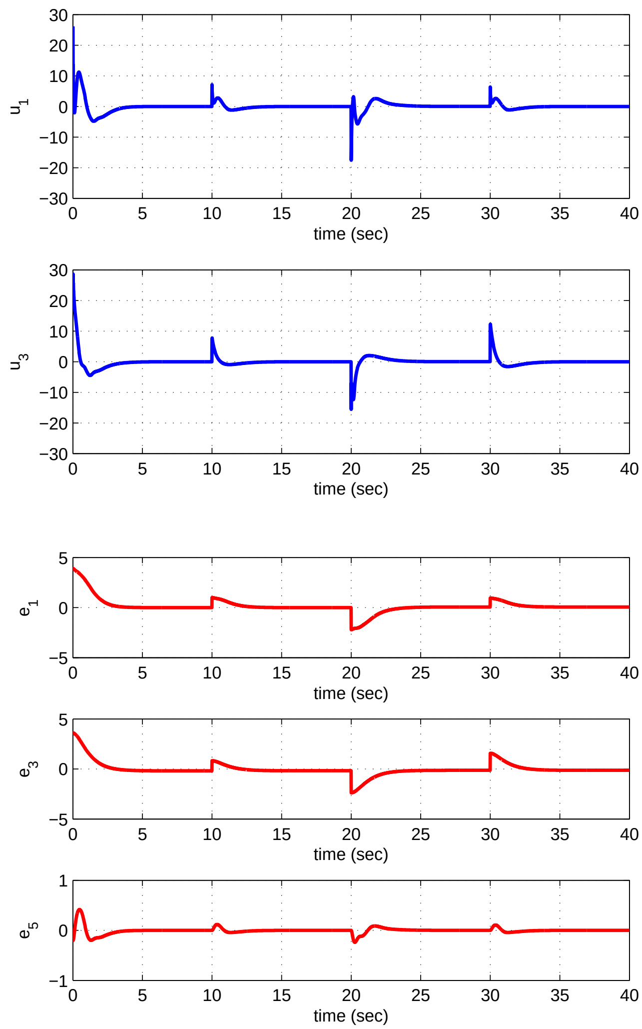

Figure 16. Tracking of setpoint 7 by the two cable-driven 3-DOF robotic crane with nonlinear optimal control: (top) variations of the control inputs of the gantry crane u_1 and u_2 (blue line), (bottom) convergence to 0 of the tracking error variables e_1, e_3 and e_5 associated with state variables $x_1 = x_R$, $x_3 = y_R$ and $x_5 = \theta$

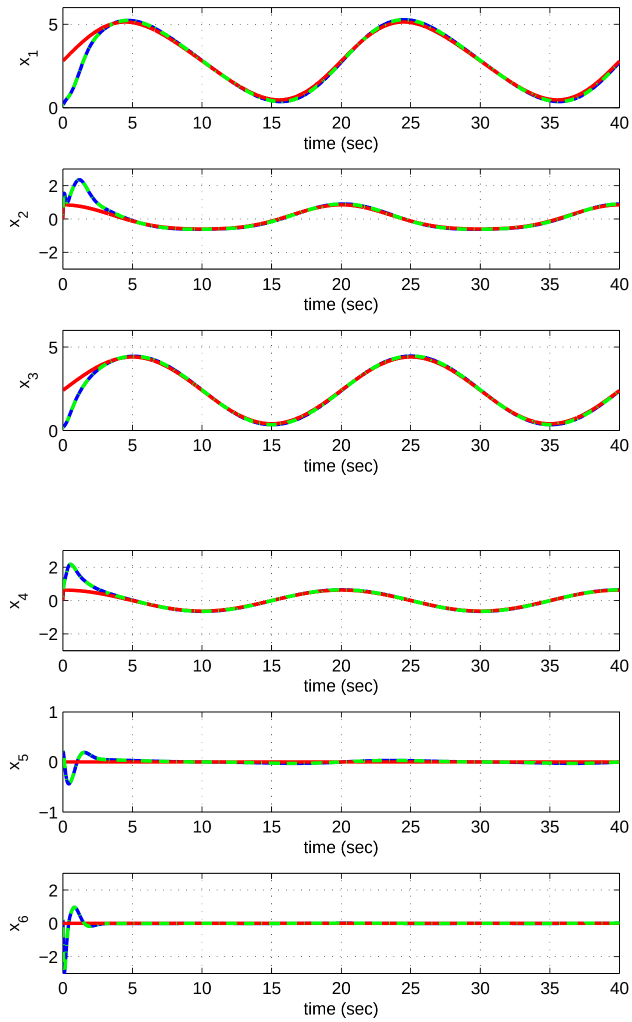

Figure 17. Tracking of setpoint 8 by the two cable-driven 3-DOF robotic crane with nonlinear optimal control: (top) tracking of setpoints (red line) by the state variables of the crane x_1 to x_3 (blue line) and estimates provided by the H-infinity Kalman Filter, (bottom) tracking of setpoints (red line) by the state variables of the crane x_4 to x_6 (blue line) and estimates provided by the H-infinity Kalman Filter

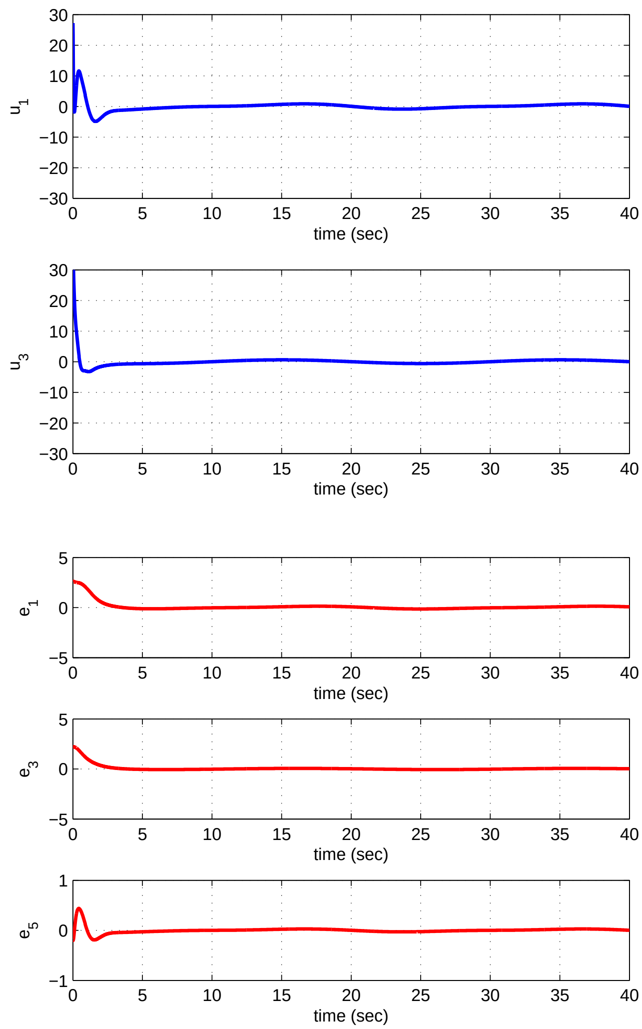

Figure 18. Tracking of setpoint 8 by the two cable-driven 3-DOF robotic crane with nonlinear optimal control: (top) variations of the control inputs of the gantry crane u_1 and u_2 (blue line), (bottom) convergence to 0 of the tracking error variables e_1, e_3 and e_5 associated with state variables $x_1 = x_R$, $x_3 = y_R$ and $x_5 = \theta$

Table I - Nonlinear optimal control						
Tracking RMSE in the disturbance-free case						
	$RMSE_{x_1}$	$RMSE_{x_2}$	$RMSE_{x_3}$	$RMSE_{x_4}$	$RMSE_{x_5}$	$RMSE_{x_6}$
test_1	0.0015	0.0000	0.0012	0.0000	0.0000	0.0000
test_2	0.0015	0.0000	0.0015	0.0000	0.0000	0.0000
test_3	0.0012	0.0000	0.0014	0.0000	0.0000	0.0000
test_4	0.0022	0.0001	0.0028	0.0002	0.0000	0.0000
test_5	0.0004	0.0001	0.0070	0.0002	0.0000	0.0000
test_6	0.0020	0.0000	0.0039	0.0002	0.0000	0.0000
test_7	0.0025	0.0001	0.0058	0.0002	0.0000	0.0000
test_8	0.0040	0.0013	0.0056	0.0006	0.0010	0.0003

Table II - Nonlinear optimal control						
Tracking RMSE in the case of disturbances						
$\Delta a\%$	$RMSE_{x_1}$	$RMSE_{x_2}$	$RMSE_{x_3}$	$RMSE_{x_4}$	$RMSE_{x_5}$	$RMSE_{x_6}$
0%	0.0012	0.0000	0.0012	0.0001	0.0000	0.0000
10%	0.0068	0.0001	0.0088	0.0001	0.0000	0.0000
20%	0.0099	0.0001	0.0121	0.0001	0.0000	0.0000
30%	0.0111	0.0001	0.0131	0.0001	0.0000	0.0000
40%	0.0125	0.0001	0.0126	0.0001	0.0000	0.0000
50%	0.0128	0.0001	0.0113	0.0001	0.0000	0.0000
60%	0.0129	0.0001	0.0004	0.0001	0.0000	0.0000

Table III - Nonlinear optimal control						
RMSE of state estimates provided by the HKF						
	$RMSE_{\hat{x}_1}$	$RMSE_{\hat{x}_2}$	$RMSE_{\hat{x}_3}$	$RMSE_{\hat{x}_4}$	$RMSE_{\hat{x}_5}$	$RMSE_{\hat{x}_6}$
test_1	0.0001	0.0009	0.0001	0.0009	0.0000	0.0000
test_2	0.0001	0.0010	0.0001	0.0010	0.0000	0.0000
test_3	0.0000	0.0008	0.0001	0.0009	0.0000	0.0000
test_4	0.0002	0.0001	0.0002	0.0020	0.0000	0.0000
test_5	0.0000	0.0003	0.0006	0.0052	0.0000	0.0000
test_6	0.0002	$9,9991$	0.0003	0.0027	0.0000	0.0000
test_7	0.0002	0.0002	0.0005	0.0043	0.0000	0.0000
test_8	0.0002	0.0001	0.0007	0.0029	0.0000	0.0000

Table IV - Nonlinear optimal control						
Convergence times T_s (sec) of the state variables						
	T_s x_1	T_s x_2	T_s x_3	T_s x_4	T_s x_5	T_s x_6
test_1	3.5	3.5	2.5	2.5	2.5	2.0
test_2	2.5	3.0	3.0	2.5	1.5	3.0
test_3	3.5	3.5	3.0	4.0	3.5	2.5
test_4	3.5	3.5	2.5	3.5	3.0	1.5
test_5	3.5	3.5	3.0	3.0	3.0	1.5
test_6	2.5	3.0	3.0	3.5	2.5	1.5
test_7	3.5	3.5	3.0	3.5	3.5	1.5
test_8	3.5	4.0	3.5	3.5	3.0	2.5

The proposed nonlinear optimal control method has clear computational advantages, when compared to fuzzy multi-model feedback control. The state-space model of the 3-DOF two-cable driven robotic crane has the state vector $x \in R^{6\times 1}$. If one substitutes the initial nonlinear model with fuzzy-weighted local models, then the aggregate number of local models and the associated number of linearization points grows exponentially with the number of the state variables. Thus, if each state variable is partitioned into 5 fuzzy sets, the total number of local models will be $5^6 = 15\,635$. Therefore, to cover sufficiently the entire state-space of the controlled system one has to use a remarkably high number of local models and has to solve an equal number of Riccati equations.

On the top of this, with the article's nonlinear optimal control approach there is need to solve only one Riccati equation in each iteration of the control algorithm. For a total number of iterations $N = 1000$ this means that one has to solve 1000 Riccati equations, which is only 6.4% of the Riccati equations that have to be solved in the case of fuzzy control with multiple local models. Consequently, there is a significant computational benefit if one uses the article's nonlinear optimal control method and the associated sequential linearization approach. It has been also confirmed that the execution time for the solution of the Riccati equation is of the order of msec and is significantly shorter than the sampling period of the sequential linearization method.

7. Conclusions

Cable-driven robotic cranes are widely used in industry, particularly in applications, in which the robot operates in large work-spaces. In this article, a nonlinear optimal control method has been proposed for the dynamic model of a two cable-driven 3-DOF cable train. Such cranes can be used in ship maintenance and repair. Using Euler-Lagrange analysis the state-space model of the robotic crane has been formulated and differential flatness properties have been proven about it. Next, the system's state-space model undergoes an approximate linearization procedure around a temporary operating point, which is updated at each sampling interval. The linearization process is based on first-order Taylor series expansion and on the computation of Jacobian matrices. For the linearized model of the crane an H-infinity feedback controller is designed.

The H-infinity controller provides the solution to the optimal control problem for the linearized equivalent dynamics of the crane under model uncertainty and perturbations.To select the gains of the H-infinity controller an algebraic Riccati equation has to be solved at each iteration of the control algorithm. The global stability properties of the control scheme have been proven through Lyapunov analysis. The proposed nonlinear optimal control method achieves fast and precise tracking of setpoints by the state variables of the robotic crane under moderate variations of the control inputs. Moreover, the method achieves all defined control objectives without the need for a change of state variables and state-space model transformations. The method is of generic use and can be applied to more types of cranes and to other underactuated robotic systems.

Acknowledgement

(a) Gerasimos Rigatos has been partially supported by Grant Ref. 311022 "Nonlinear optimal and flatness-based control methods" of the Unit of Industrial Automation, Industrial Systems Institute, Greece; (b) Mohammed Al-Numay acknowledges the financial support from the Researchers Supporting Project Number (RSP2025R150), King Saud University, Riyadh, Saudi Arabia.

Data related statement

Data about the article's results can be made available by the authors upon reasonable request.

References

Bahadure, S., Venkatesh, C. and Kazi, F. (2012) Structure preserving optimal control of 2D SpiderCrane. *IEEE SysCon 2012, Intl. Conf. on Systems and Control*, Vancouver, Canada.

Barbazza, L., Zanotto, D., Rosati, G. and Agrawal, S.K. (2017) Design and optimal control of an underactuated cable-driven micro-macro robot. *IEEE Robotics an Automation Letters*, **2**, 2, 896-903.

Basseville, M. and Nikiforov, I. (1993) *Detection of abrupt changes: Theory and Applications.* Prentice-Hall.

Brogliato, B. (2023) Modelling analysis and control of robot-object nonsmooth underactuated Lagrangian systems: A tutorial overview and perspectives. *Annual Reviews in Control*, Elsevier, **55**, 297-337.

Buccieri, D., Mullhaupt, P. and Bonvin, D. (2005) SpiderCrane: Model and properties of a fast weight handling equipment. *IFAC 16th Triennial World Congress*, Prague, Czech Republic.

Buccieri, D., Sanchez, J., Dormido, S., Mullhaupt, P. and Bonvin, D. (2005) Interactive 3D Simulation of Flat Systems: The SpiderCrane as a case study. *IEEE CDC 2005, IEEE 44th Intl. Conference on Decision and Control*, Seville, Spain, Dec. 3.

Choukchou-Braham, A., Cherki, B., Djemai M. and Busawon, K. (2014) *Analysis and Control of Underactuated Mechanical Systems*. Springer.

Étienne, L., Cardou, P., Métillon, M. and Caro, S. (2022) Design of a Planar Cable-Driven Parallel Crane Without Parasitic Tilt. *ASME Journal of Mechanisms and Robotics*, **14**, 4, 041006, 1-11.

Gamboa Penaloza, E. A., Caballero, P. D. P., Lestor, L. A. and de Lima, S. (2025) Development of a four cable-driven parallel robot for execution of complex tasks in closed environments. *Intl. Journal of Dynamics and Control*, Springer, **13**, 83, 1-14.

Gogte, G., Venkatesh, C., Kazi, F., Singh, N. M. and Pasumarthy, R. (2012) Passivity-based control of underactuated 2D SpiderCrane manipulator. *MTNS 2012, 20th Intl. Symp. on Mathematical Theory, Networks and Systems*, Melbourne, Australia, July 2012.

Harandi, M .R. J. and Taghirad, H. D. (2021) On the matching equations of kinetic energy shaping in IDA-PBC. *Journal of the Franklin Institute*, Elsevier, **358**, 8639-8655.

Harandi, M. R. J. and Taghirad, H. D. (2021) Adaptive inerconnection and damping assignment passivity-based control for an underactuated cable-driven robot. *Intl. Journal of Adaptive Control and Signal Processing*, J. Wiley, **35**, 2487-2498.

Harandi, M. R. J. and Taghirad, H. D. (2023) Stabilization of a class of underactuated parallel robots via energy shaping: Application to cable-driven manipulators. *Automatica*, Elsevier, **156**, 111201-111205.

Harandi, M. R. J., Khalilpour, S. A. and Taghirad, H. D. (2023) Adaptive energy-shaping control of a 3-DOF underactuated cable-driven parallel robot. *IEEE Transactions on Industrial Informatics*, **19**, 6, 7552-7560.

Harandi, M. R. J., Namvar, M. and Taghirad, H. D. (2023) Stabilization of robots with actuator constraints via interconnection and damping assignment. *IEEE Transactions on Control Systems Technology*, 1-8.

Hosseini, H. J., Khalilpour, S. A. and Taghirad, H. D. (2021) Practical robust nonlinear PD controller for cable-driven parallel manupulators. *Nonlinear Dynamics*, Springer, **106**, 405-424.

Huang, S. W., Bak, J. H., Yoon, J. Y., Park, J. H. and Park, J. O. (2016) Trajectory generation to suppress oscillations in under-constrained cable-driven parallel robots. *Journal of Mechanical Science and Technology*, Springer, **30**, 12, 5689-5697.

Huang, S. W., Kim, D. H., Park, J. and Park, J. H. (2022) Equilibrium configuration analysis and equilibrium-based trajectory generation method for under-constrained cable-driven parallel robot. *IEEE Acceess*, **10**, 112134-112149.

Ida, E., Bruckmann, T. and Carricato, M. (2016) Rest-to-rest trajectory planning for underactuated cable-driven parallel robots. *IEEE Transactions on Robotics*, **35**, 6, 728-738.

Kamath, A. K., Kazi, F. and Singh, N. M. (2010) Dynamics and Control of 2D SpiderCrane: A RHC Approach. *IFAC MTNS 2010. Proc. of the 19th Intl. Symposium on Mathematical Theory of Networks and Systems*, Budapest, Hungary, July 2010.

Kazi, F., Banavar, R. N., Mullhaupt, P. and Bonvin, D. (2008) Stabilization of a 2D Spider crane mechamism using damping assignment passivity-based control. *IFAC WC 2008, The 17th IFAC World Congress*, Seoul, Korea, July 2008.

Kazi, F., Mullhaupt, P., Banavar, R. M. and Bonvin, D. (2009) Dynamics and control of 2D Spider Crane: A Lie-Backlund approach. *Proc. ECC 2009, European Control Conference*, Budapest, Hungary, Aug. 2009.

Li, Z., Shang, W. and Zhang, B. (2023) Hybrid impendance control of cable-driven parallel robots using adaptive friction compensation. *IEEE Transactions on Industrial Electronics*, **72**, 1, 710-713.

Li, X., Kui, Q., Yao, W. and Yu, L. (2025) Robust parallel cooperate control of cable-driven robot system via adaptive integral sliding mode. *IEEE Robotics and Automation Letters*, **10**, 6, 5433-5440.

Lucarini, B., Ida, E. and Carricato, M. (2025) Point-to-point trajectory planning for underactuateed cable-driven parallel robots using input shaping: Preliminary results. In: A. Pott and T. Bruckmann, eds., *Cable-Driven Parallel Robots (CableCon 2025)*, Springer.

Mehra, R., Satpute, S., Kazi, F. and Singh, N. M. (2012) Passivity-based control of stochastic mechanical systems. *IEEE ICARCV 2012, IEEE 2012 12th Intl. Conf. on Control, Automation, Robotics and Vision*, Guangzhou, China, Dec. 2012.

Mehra, R., Satputo, S. G., Kazi, F. and Singh, N. M. (2017) Control of a class of underactuated mechanical systems obviating matching conditions. *Automatica*, Elsevier, **86**, 98-103.

Mejari, M., Gupta, A., Ketkar, V., Datar, M., Singh, N. and Kazi, F. (2014) Stabilization of 2D SpiderCrane with non-convex state constraints using MPC. *IFAC Intl. Conf. on Advances in Control and Optimizationof Dynamical Systems*, Kanpur, India, March 2014.

Mojallizadeh, M. R., Brogliato, B. and Prieur, C. (2023) Modelling and control of overhead cranes: A tutorial overview and perspectives. *Annual Reviews in Control*, Elsevier, 100877-100910.

Nurkanovic, A., Albrecht, S., Brogliato, B. and Diehl, M. (2023) The time-freezing reformulation for numerical optimal control of complementary Lagrangian systems with state jumps. *Automatica*, Elsevier, 158, 111295-111308.

Pivo, G., Richiedei, R. and Trevisani, A. (2025) Model inversion for trajectory contol of reconfigurable underactuated cable-driven parallel robots. *Nonlinear Dynamics*, Springer, **1133**, 8697-8712.

Rigatos, G. G. and Tzafestas, S. G. (2007) Extended Kalman Filtering for Fuzzy Modelling and Multi-Sensor Fusion. *Mathematical and Computer Modelling of Dynamical Systems*, Taylor & Francis, **13**, 251-266.

Rigatos, G. and Zhang, Q. (2009) Fuzzy model validation using the local statistical approach. *Fuzzy Sets and Systems*, Elsevier, **60**, 7, 882-904.

Rigatos, G. (2016) *Nonlinear Control and Filtering Using Differential Flatnesss Theory Approaches: Applications to Electromechanical Systems*. Springer.

Rigatos, G. and Busawon, K. (2018) *Robotic Manipulators and Vehicles: Control, Estimation and Filtering*. Springer.

Rigatos, G. and Karapanou, E. (2020) *Advances in Applied Nonlinear Optimal Control*. Cambridge Scholars Publishing.

Rigatos, G., Abbaszadeh, M. and Siano, P. (2022) *Control and Estimation of Dynamical Nonlinear and Partial Differential Equation Systems: Theory and Applications*. IET Publications.

Rigatos, G., Abbaszadeh, M., Hamida, M. A. and Siano, P. (2024) *Intelligent Control for Electric Power Systems and Electric Vehicles*. CRC Publications.

Romero, J. G. and Ortega, R. (2015) Two globally convergent adaptive speed observers for mechanical systems. *Automatica*, Elsevier, **60**, 7-11.

Romero, J. C., Donaire, A., Ortega, R. and Borja, P. (2018) Global stabilization of underactuated mechanical systems via PID passivity-based control, *Automatica*, Elsevier, **98**, 178-185.

Romero, J. D, Gandarilla, I., Sanibanez, V. and Yi, B. (2022) A constructive procedure for orbital stabilization of a class of underactuated mechanical systems. *IEEE Transactions on Control Systems Technology*, **30**, 6, 2698-2706.

Seifired, R. (2013) Dynamics of Underactuated Multibody Systems Modeling. *Control and Optimal Design*, 1st edn., Springer.

Sun, H., Zhang, R., Ji, R., Tong, X. and Ge, S. S. (2025) Tracking control with adjustable trajectory envelope for cable-driven robots. *IEEE Transactions on Industrial Electronics*, **72**, 7, 7128-7188.

Toussaint, G. J., Basar, T. and Bullo, F. (2000) H_∞ optimal tracking control techniques for nonlinear underactuated systems. In: *Proc. IEEE CDC 2000, 39th IEEE Conference on Decision and Control*, Sydney Australia.

Zhang, B., Shang, W. and Cong, S. (2025) Synchronous impedance control of cable-driven parallel robots with3external interactions. *IEEE / ASME Transactions on Mechatronics*, 1-15.

Zhu, B., Zhao, T., Tang, Z., Ding, S. and Li, E. (2023) Hierarchical coupling control of cable-driven multi-loop crane for underactuated positioning. *Intl. Journal of Mechanical Sciences*, Elsevier, **259**, 108620-108645.

Zoso, N. and Gosselin, C. (2012) Point-to-point motion planning of a parallel 3-DOF underactuated cable-suspended robot. *IEEE Intl. Conf. on Robotics and Automation*, Saint Paul, Minnesota, May 2012.

Appendix: Jacobian matrices of the 3-DOF two-cable driven robotic crane

In what follows, the computation of Jacobian matrix $\nabla_x f(x) \mid_{(x^*,u^*)}$ is presented.

(1) First row of the Jacobian matrix $\nabla_x f(x) \mid_{(x^*,u^*)}$: $\frac{\partial f_1}{\partial x_1}=0$, $\frac{\partial f_1}{\partial x_2}=1$, $\frac{\partial f_1}{\partial x_3}=0$, $\frac{\partial f_1}{\partial x_4}=0$, $\frac{\partial f_1}{\partial x_5}=0$ and $\frac{\partial f_1}{\partial x_6}=0$.

(2) Second row of the Jacobian matrix $\nabla_x f(x) \mid_{(x^*,u^*)}$: It holds that

$$f_2 = \frac{f_{2,num}}{f_{2,den}} = \frac{-M_{11}C_1 + M_{21}C_2 - M_{31}G_3}{detM} \ . \tag{72}$$

It holds that for $1,2,\cdots,6$

$$\frac{\partial f_2}{\partial x_i} = \frac{\frac{\partial f_{2,num}}{\partial x_i} detM - f_{2,num}\frac{\partial detM}{\partial x_i}}{detM^2} \tag{73}$$

where for $1,2,\cdots,6$

$$\frac{\partial f_{2,num}}{\partial x_i} = -\frac{\partial M_{11}}{\partial x_i}C_1 - M_{11}\frac{\partial C_1}{\partial x_i} + \frac{\partial M_{11}}{\partial x_i}C_2 + M_{21}\frac{\partial C_2}{\partial x_i} - \frac{\partial M_{31}}{\partial x_i}G_3 - M_{31}\frac{\partial G_3}{\partial x_i} \tag{74}$$

and also for $1,2,\cdots,6$

$$\frac{\partial detM}{\partial x_i}=(M+m)\frac{\partial M_{11}}{\partial x_i}-(mL_3sin(x_5))M_{13}+mL_3cos(x_5)\frac{\partial M_{13}}{\partial x_i}\ . \quad (75)$$

(3) Third row of the Jacobian matrix $\nabla_x f(x)\mid_{(x^*,u^*)}$: $\frac{\partial f_3}{\partial x_1}=0$, $\frac{\partial f_3}{\partial x_2}=0$, $\frac{\partial f_3}{\partial x_3}=0$, $\frac{\partial f_3}{\partial x_4}=1$, $\frac{\partial f_3}{\partial x_5}=0$ and $\frac{\partial f_3}{\partial x_6}=0$.

(4) Fourth row of the Jacobian matrix $\nabla_x f(x)\mid_{(x^*,u^*)}$: It holds that

$$f_4=\frac{f_{4,num}}{f_{4,den}}=\frac{M_{12}C_1-M_{22}C_2+M_{32}G_3}{detM}\ . \quad (76)$$

It holds that for $i=1,2,\cdots,6$

$$\frac{\partial f_4}{\partial x_i}=\frac{\frac{\partial f_{4,num}}{\partial x_i}detM-f_{4,num}\frac{\partial detM}{\partial x_i}}{detM^2} \quad (77)$$

where for $i=1,2,\cdots,6$

$$\frac{\partial f_{4,num}}{\partial x_i}=\frac{\partial M_{12}}{\partial x_i}C_1+M_{12}\frac{\partial C_1}{\partial x_i}-\frac{\partial M_{22}}{\partial x_i}C_2-M_{22}\frac{\partial C_2}{\partial x_i}+\frac{\partial M_{32}}{\partial x_i}G_3+M_{32}\frac{\partial G_3}{\partial x_i}. \quad (78)$$

(5) Fifth row of the Jacobian matrix $\nabla_x f(x)\mid_{(x^*,u^*)}$: $\frac{\partial f_5|}{\partial x_1}=0$, $\frac{\partial f_5}{\partial x_2}=0$, $\frac{\partial f_5}{\partial x_3}=0$, $\frac{\partial f_5}{\partial x_4}=0$, $\frac{\partial f_3}{\partial x_5}=0$ and $\frac{\partial f_5}{\partial x_6}=1$.

(6) Sixth row of the Jacobian matrix $\nabla_x f(x)\mid_{(x^*,u^*)}$: It holds that

$$f_6=\frac{f_{6,num}}{f_{6,den}}=\frac{-M_{13}C_1+M_{23}C_2-M_{33}G_3}{detM}\ . \quad (79)$$

It holds that for $1,2,\cdots,6$

$$\frac{\partial f_6}{\partial x_i}=\frac{\frac{\partial f_{6,num}}{\partial x_i}detM-f_{6,num}\frac{\partial detM}{\partial x_i}}{detM^2} \quad (80)$$

where for $1,2,\cdots,6$

$$\frac{\partial f_{6,num}}{\partial x_i}=\frac{-\partial M_{13}}{\partial x_i}C_1-M_{13}\frac{\partial C_1}{\partial x_i}+\frac{\partial M_{23}}{\partial x_i}C_2+M_{23}\frac{\partial C_2}{\partial x_i}-\frac{\partial M_{33}}{\partial x_i}G_3-M_{33}\frac{\partial G_3}{\partial x_i}\ . \quad (81)$$

Following this, the Jacobian matrix $\nabla_x g_1(x)\mid_{(x^*,u^*)}$ computation is presented:

(1) First row of the Jacobian matrix $\nabla_x g_1(x)\mid_{(x^*,u^*)}$: $\frac{\partial g_{11}}{\partial x_i}=0$. for $i=1,2,\cdots,6$.

(2) Second row of the Jacobian matrix $\nabla_x g_1(x) \mid_{(x^*,u^*)}$: It holds that for $i = 1, 2, \cdots, 6$

$$\frac{\partial g_{21}}{\partial x_i} = \frac{\frac{\partial M_{11}}{\partial x_i} detM - M_{11} \frac{\partial detM}{\partial x_i}}{detM^2} \ . \tag{82}$$

(3) Third row of the Jacobian matrix $\nabla_x g_1(x) \mid_{(x^*,u^*)}$: $\frac{\partial g_{31}}{\partial x_i} = 0$. for $i = 1, 2, \cdots, 6$.

(4) Fourth row of the Jacobian matrix $\nabla_x g_1(x) \mid_{(x^*,u^*)}$: It holds that for $i = 1, 2, \cdots, 6$

$$\frac{\partial g_{41}}{\partial x_i} = \frac{-\frac{\partial M_{12}}{\partial x_i} detM + M_{12} \frac{\partial detM}{\partial x_i}}{detM^2} \ . \tag{83}$$

(5) Fifth row of the Jacobian matrix $\nabla_x g_1(x) \mid_{(x^*,u^*)}$: $\frac{\partial g_{51}}{\partial x_i} = 0$, for $i = 1, 2, \cdots, 6$.

(6) Sixth row of the Jacobian matrix $\nabla_x g_1(x) \mid_{(x^*,u^*)}$: It holds that for $i = 1, 2, \cdots, 6$

$$\frac{\partial g_{61}}{\partial x_i} = \frac{\frac{\partial M_{13}}{\partial x_i} detM - M_{13} \frac{\partial detM}{\partial x_i}}{detM^2} \ . \tag{84}$$

Now, the Jacobian matrix $\nabla_x g_2(x) \mid_{(x^*,u^*)}$ is computed as follows:

(1) First row of the Jacobian matrix $\nabla_x g_2(x) \mid_{(x^*,u^*)}$: $\frac{\partial g_{12}}{\partial x_i} = 0$. for $i = 1, 2, \cdots, 6$.

(2) Second row of the Jacobian matrix $\nabla_x g_2(x) \mid_{(x^*,u^*)}$: It holds that for $i = 1, 2, \cdots, 6$

$$\frac{\partial g_{22}}{\partial x_i} = \frac{-\frac{\partial M_{12}}{\partial x_i} detM + M_{12} \frac{\partial detM}{\partial x_i}}{detM^2} \ . \tag{85}$$

(3) Third row of the Jacobian matrix $\nabla_x g_2(x) \mid_{(x^*,u^*)}$: $\frac{\partial g_{32}}{\partial x_i} = 0$. for $i = 1, 2, \cdots, 6$.

(4) Fourth row of the Jacobian matrix $\nabla_x g_2(x) \mid_{(x^*,u^*)}$: It holds that for $i = 1, 2, \cdots, 6$

$$\frac{\partial g_{42}}{\partial x_i} = \frac{\frac{\partial M_{22}}{\partial x_i} detM - M_{22} \frac{\partial detM}{\partial x_i}}{detM^2} \ . \tag{86}$$

(5) Fifth row of the Jacobian matrix $\nabla_x g_2(x) \mid_{(x^*,u^*)}$: $\frac{\partial g_{52}}{\partial x_i} = 0$, for $i = 1, 2, \cdots, 6$.

(6) Sixth row of the Jacobian matrix $\nabla_x g_2(x) \mid_{(x^*,u^*)}$: It holds that for $i = 1, 2, \cdots, 6$

$$\frac{\partial g_{62}}{\partial x_i} = \frac{-\frac{\partial M_{32}}{\partial x_i} detM + M_{32}\frac{\partial detM}{\partial x_i}}{detM^2} \ . \tag{87}$$

Computation of the partial derivatives of the sub-determinants of the inertia matrix:

M_{11} It holds that $\frac{\partial M_{11}}{\partial x_i} = 0$ for $i = 1, 2, \cdots, 6$ and $i \neq 5$ while $\frac{\partial M_{11}}{\partial x_5} = -(ML_3)^2 sin(x_5)cos(x_5)$.

M_{12} Additionally, it holds that $\frac{\partial M_{12}}{\partial x_i} = 0$ for $i = 1, 2, \cdots, 6$ and $i \neq 5$ while $\frac{\partial M_{12}}{\partial x_5} = -(mL_3)^2[cos(x_5)^2 - sin(x_5)^2]$.

M_{13} Moreover, it holds that $\frac{\partial M_{13}}{\partial x_i} = 0$ for $i = 1, 2, \cdots, 6$ and $i \neq 5$ while $\frac{\partial M_{13}}{\partial x_5} = (M + m)(mL_3)sin(x_5)$.

M_{21} Furthermore, one has that $\frac{\partial M_{21}}{\partial x_i} = 0$ for $i = 1, 2, \cdots, 6$ and $i \neq 5$ while $\frac{\partial M_{21}}{\partial x_5} = -(mL_3)^2[cos(x_5)^2 - sin(x_5)^2]$.

M_{22} Additionally, it holds that $\frac{\partial M_{22}}{\partial x_i} = 0$ for $i = 1, 2, \cdots, 6$ and $i \neq 5$ while $\frac{\partial M_{22}}{\partial x_5} = 2(mL_3)^2 sin(x_5)cos(x_5)$.

M_{23} Moreover, it holds that $\frac{\partial M_{23}}{\partial x_i} = 0$ for $i = 1, 2, \cdots, 6$ and $i \neq 5$ while $\frac{\partial M_{23}}{\partial x_5} = (M + m)(mL_3)cos(x_5)$.

M_{31} Furthermore, one has that $\frac{\partial M_{31}}{\partial x_i} = 0$ for $i = 1, 2, \cdots, 6$ and $i \neq 5$ while $\frac{\partial M_{31}}{\partial x_5} = (M + m)(mL_3)sin(x_5)$.

M_{32} Moreover, it holds that $\frac{\partial M_{32}}{\partial x_i} = 0$ for $i = 1, 2, \cdots, 6$ and $i \neq 5$ while $\frac{\partial M_{32}}{\partial x_5} = (M + m)(mL_3)cos(x_5)$.

M_{33} Finally, it holds that $\frac{\partial M_{33}}{\partial x_i} = 0$ for $i = 1, 2, \cdots, 6$.

Computation of the partial derivatives of the non-zero elements of the Coriolis forces vector $C(q,\dot{q})$:

It holds that $\frac{\partial C_1}{\partial x_1}=0$, $\frac{\partial C_1}{\partial x_2}=0$, $\frac{\partial C_1}{\partial x_3}=0$, $\frac{\partial C_1}{\partial x_4}=0$, $\frac{\partial C_1}{\partial x_5}=-(mL_3cos(x_5))x_6^2$, and $\frac{\partial C_1}{\partial x_6}=-2(mL_3sin(x_5))x_6$.

Moreover, it holds that $\frac{\partial C_2}{\partial x_1}=0$, $\frac{\partial C_2}{\partial x_2}=0$, $\frac{\partial C_2}{\partial x_3}=0$, $\frac{\partial C_2}{\partial x_4}=0$, $\frac{\partial C_2}{\partial x_5}=-(mL_3sin(x_5))x_6^2$, and $\frac{\partial C_2}{\partial x_6}=2(mL_3cos(x_5))x_6$.

Computation of the partial derivatives of the non-zero elements of the gravitational forces vector $G(q)$:

It holds that $\frac{\partial G_3}{\partial x_1}=0$, $\frac{\partial G_3}{\partial x_2}=0$, $\frac{\partial G_3}{\partial x_3}=0$, $\frac{\partial G_3}{\partial x_4}=0$, $\frac{\partial G_3}{\partial x_5}=(mgL_3cos(x_5))$, and $\frac{\partial G_3}{\partial x_6}=0$.